FBXO45-MYCBP2 regulates mitotic cell fate by targeting FBXW7 for degradation

Kai T. Richter, Yvonne T. Kschonsak[#], Barbara Vodicska[#] and Ingrid Hoffmann*

Cell Cycle Control and Carcinogenesis, F045, German Cancer Research Center, DKFZ, Im Neuenheimer Feld 242, 69120 Heidelberg, Germany

[#]These authors contributed equally

*Correspondence: Ingrid.Hoffmann@dkfz.de

SUMMARY

Cell fate decision upon prolonged mitotic arrest induced by microtubule targeting agents depends on the activity of the tumor suppressor and F-box protein FBXW7. FBXW7 promotes mitotic cell death and prevents premature escape from mitosis through mitotic slippage. Mitotic slippage is a process that can cause chemoresistance and tumor relapse. Therefore, understanding the mechanisms that regulate the balance between mitotic cell death and mitotic slippage is an important task. Here we report that FBXW7 protein levels markedly decline during extended mitotic arrest. FBXO45 binds to a conserved acidic N-terminal motif of FBXW7 specifically under a prolonged delay in mitosis, leading to ubiquitylation and subsequent proteasomal degradation of FBXW7 by the FBXO45-MYCBP2 E3 ubiquitin ligase. Moreover, we find that FBXO45-MYCBP2 counteracts FBXW7 in that it promotes mitotic slippage and prevents cell death in mitosis. Targeting this interaction represents a promising strategy to prevent chemotherapy resistance.

Key words: FBXW7, ubiquitylation, proteasome, FBXO45, MYCBP2, mitotic slippage, cell fate decision, SCF, mitotic cell death

INTRODUCTION

The attachment of a single ubiquitin molecule or a polyubiquitin chain to a eukaryotic protein is an essential signaling event that can profoundly affect the fate of the target protein. For example, the ubiquitin-proteasome system controls protein degradation in a broad array of cellular processes [1]. Cancer cells often contain mutations targeting ubiquitin-mediated proteolysis that lead to tumorigenesis. FBXW7, an F-box protein and substrate receptor for the SCF (SKP1-CUL1-F-box protein) E3 ubiquitin ligase complex, acts as a tumor suppressor and is mutated or deleted in a variety of human cancers [2]. FBXW7 exerts its anti-tumor activity through destruction of key oncoproteins, including JUN [3] [4], MYC [5] [6], Cyclin E [7] [8] [9] and Notch1 [10] [11].

The abundance of F-box proteins including FBXW7 is controlled by ubiquitylation and degradation in an autocatalytic reaction within the SCF complex [12]. FBXW7 autoubiquitylation can be regulated by Glomulin (GLMN), a protein that binds to RBX1 leading to inhibition of SCF activity, thereby increasing FBXW7 protein levels [13] [14]. The only ubiquitin ligase known to date involved in regulating FBXW7 levels in neurons is Parkin. However, this regulation has only been observed for the FBXW7β isoform [15]. It has also been shown that PLK2-kinase dependent phosphorylation of FBXW7 at S176 leads to its ubiquitin-mediated degradation and stabilization of Cyclin E [16].

Accurate spindle function is crucial for a successful mitosis. Perturbation of microtubule dynamics leads to sustained activation of the spindle assembly checkpoint (SAC) [17]. The SAC delays exit from mitosis by preventing the anaphase-promoting complex/cyclosome (APC/C) mediated proteolysis of Cyclin B1. Anti-cancer chemotherapeutics including vinca alkaloids or taxanes target microtubules and are successfully used in the clinics to treat multiple types of cancer. Anti-microtubule drugs cause an arrest or prolonged delay in mitosis followed by mitotic cell death. On the other hand, slow degradation of Cyclin B1 during a prolonged mitotic arrest can cause cells to prematurely exit from mitosis, a process called mitotic slippage [18]. During mitotic slippage, cells do not undergo proper chromosome segregation and cytokinesis. Most of the resulting tetraploid cells either undergo cell death after mitosis or arrest

in interphase. However, depending on the p53 status of these cells, they may continue to proliferate as genomically unstable cells. This can lead to chemoresistance, thereby limiting the therapeutic use of anti-microtubule drugs [19] [20]. FBXW7 is a known regulator of mitotic cell fate. Upon mitotic arrest, FBXW7 promotes mitotic cell death and prevents mitotic slippage [21] [22].

FBXO45 (FSN-1 in *C. elegans*; DFsn in *Drosophila melanogaster*) is an evolutionary conserved F-box protein. FBXO45 is atypical in that it binds to SKP1 via its F-box motif, but recruits an alternate RING-finger protein known as MYCBP2, a member of the PHR (PAM/Highwire/RPM-1) protein family and E3 ubiquitin ligase. MYCBP2 was shown to have important functions in developmental processes, such as axon termination and synapse formation, as well as axon degeneration (reviewed by [23] [24]). FBXO45 contains a conserved F-box domain and a SPRY domain, which recruits substrates to the ubiquitin ligase complex [25] [26]. FBXO45-MYCBP2 has been linked to the proteasomal degradation of a few targets including the DLK-1 and p38 MAP kinase pathway [27] and the nicotinamide-nucleotide adenylyltransferase family member NMNAT [28].

Here we report the identification of the E3 ligase FBXO45-MYCBP2 as a regulator of FBXW7 abundance during prolonged mitotic arrest induced by spindle poisons. FBXO45 binds to a conserved acidic N-terminal region of FBXW7. Depletion of FBXO45 leads to stabilization of FBXW7 protein upon mitotic arrest. Ubiquitylation of FBXW7 by FBXO45-MYCBP2 induces its proteasomal degradation inducing an increase in mitotic slippage and prevention of mitotic cell death.

RESULTS AND DISCUSSION

Prolonged mitotic arrest leads to reduced FBXW7 protein levels

The SCF-FBXW7 complex acts as a key factor determining sensitivity to anti-mitotic drugs in cancer by inducing mitotic cell death and preventing mitotic slippage [29] [22] [21]. As mitotic slippage frequently occurs under prolonged mitotic arrest, it is conceivable that this could be induced by a decrease in FBXW7 protein levels. To address this, we analyzed protein levels of the

103 ubiquitously expressed α-isoform of FBXW7 in mitotic HeLa cells at different
104 time points after induction of mitotic arrest. We observed a slow but gradual
105 decrease in the amount of FBXW7 protein during prolonged mitotic arrest
106 (Figure 1A). The dynamics of this decrease was similar to the decay of two
107 other regulators of mitotic cell fate, Cyclin B1 and MCL-1 [18] [30]. Moreover,
108 the decay of FBXW7, Cyclin B1 and MCL-1 was prevented by the addition of
109 the proteasomal inhibitor MG132 (Figure 1B). We therefore anticipated that
110 FBXW7 protein levels could be decreased in response to proteasomal protein
111 degradation. To identify proteins that regulate SCF-FBXW7 protein levels we
112 made use of an unbiased screen where we aimed at identifying FBXW7
113 binding proteins. We expressed Flag-FBXW7α in HEK-293T cells, FBXW7α
114 complexes were immunoprecipitated and subsequent mass spectrometrical
115 analysis was performed. Among the identified peptides were sequences
116 corresponding to FBXO45 and MYCBP2, along with SCF components and
117 known substrates of FBXW7 including MYC, Notch1/2 and members of the
118 mediator complex (Figure 1C, Table S1). Interestingly, FBXO45 and MYCBP2
119 have previously been identified in other screens for FBXW7 interacting
120 proteins [31] [32]. They have also been described to form an SCF-like E3
121 ubiquitin ligase complex [33]. We therefore analyzed whether FBXO45-
122 MYCBP2 is the ubiquitin ligase that regulates FBXW7 protein levels under
123 prolonged mitotic arrest.
124
125 **The FBXO45-MYCBP2 complex binds to a conserved N-terminal motif in**
126 **FBXW7α**
127 First, we checked whether FBXO45 and FBXW7α bind to each other and
128 found that Flag-FBXO45 was able to co-immunoprecipitate endogenous
129 FBXW7α (Figure 2A) and vice versa Flag-FBXW7α co-immunoprecipitated
130 endogenous FBXO45 (Figure 2B). To confirm the specificity of the binding
131 between FBXW7α and FBXO45, several other F-box and DCAF substrate
132 receptors were expressed and immunoprecipitated. No interaction was
133 detected between FBXO45/FBXW7α and the control proteins suggesting that
134 the binding of FBXO45 and FBXW7α was specific (Figures 2A-B). FBXW7
135 occurs in three isoforms, FBXW7α, FBXW7β and FBXW7γ, that differ in
136 subcellular localization and their N-terminal domain. FBXW7α is thought to

137 perform most FBXW7 functions [2]. To identify the binding site of FBXO45
138 within FBXW7 we generated different FBXW7α truncated versions and found
139 that aa106-126 in the N-terminal domain of FBXW7α were required for
140 FBXO45 binding (Figures EV1A-D). Co-immunoprecipitation experiments
141 using full-length Flag-FBXW7α or a Flag-FBXW7αΔ106-126 mutant showed
142 that FBXW7αΔ106-126 failed to bind FBXO45 and MYCBP2 (Figure 2C). This
143 could be confirmed by the fact that FBXO45 only interacted with FBXW7α but
144 not with the other two isoforms, FBXW7β or FBXW7γ (Figure EV1E), that lack
145 the FBXW7α-specific N-terminal domain [34] again suggesting FBXW7α
146 specifically binds FBXO45. Interestingly, the N-terminal stretch within the
147 FBXW7α isoform (aa106-126) harbors conserved acidic amino acid residues
148 as a potential FBXO45 interaction domain (Figure 2D). On the other hand, we
149 identified the central domain of MYCBP2 (aa1951-2950) to be responsible for
150 FBXW7α binding (Figures EV2A-B). As this domain also contains the
151 FBXO45 interaction site of MYCBP2, we hypothesized that FBXO45 could be
152 the direct interaction partner of FBXW7α within the FBXO45-MYCBP2
153 complex. Analysis of binding between purified MBP-tagged N-terminal domain
154 of FBXW7α (MBP-FBXW7α-N167) and *in vitro* translated [^{35}S]-FBXO45 or
155 [^{35}S]-MYCBP2(1951-2950) showed that FBXW7α directly binds to FBXO45
156 but not to MYCBP2 (Figure 2E). Furthermore, using sequential co-
157 immunoprecipitation experiments we showed that FBXW7α exists in a
158 complex with FBXO45 and MYCBP2 (Figure 2F).
159 For some but not all F-box proteins it has been demonstrated that
160 phosphorylation of their specific substrates is required for binding [35]. We
161 have previously shown that phosphorylation of FBXW7 by PLK2 leads to
162 destabilization of the F-box protein [16]. However, as shown in Figure EV2C,
163 inhibition of PLK2 by the small molecule inhibitor BI2536 that targets both
164 PLK1 and PLK2 kinases did not impair the binding between FBXO45 and
165 FBXW7. Moreover, overexpression of GFP-PLK2 did not promote the
166 interaction (Figure EV2D). Our data therefore suggest that the FBXW7α-
167 FBXO45 interaction is independent of phosphorylation by PLK2.
168 Together, these results show that the FBXO45-MYCBP2 complex interacts
169 with a conserved acidic stretch within the N-terminal domain of FBXW7α.
170

171 **FBXO45-MYCBP2 targets FBXW7α for degradation specifically during**
172 **mitotic arrest**
173 As FBXW7α is predominantly found in the nucleus [36] whereas FBXO45 and
174 MYCBP2 are cytosolic proteins [25] [37] (Figure 3A), a possible interaction
175 between these proteins may occur in mitosis upon nuclear envelope
176 breakdown, when the contents of the cell nucleus are released into the
177 cytoplasm. As FBXO45 is likely to be the substrate binding factor we analyzed
178 the interaction between Flag-FBXO45 and endogenous FBXW7α in
179 asynchronous and mitotic HeLa cells. We specifically prepared the cell
180 extracts for the experiment shown in Figure 3B under conditions where the
181 nucleus remains intact in asynchronous cells. Interestingly, FBXW7α was
182 specifically found in co-immunoprecipitation with Flag-FBXO45 in mitotic cells
183 (Figure 3B). Furthermore, we noticed an increase in FBXW7α protein levels
184 upon siRNA-mediated downregulation of FBXO45. This effect could only be
185 observed in cells under a prolonged mitotic arrest but not in cells passing
186 through an unperturbed mitosis. In addition, the effect was not observed in
187 asynchronous cells (Figures 3C and EV3A-B). On the other hand, FBXW7
188 downregulation had no effect on FBXO45 protein levels (Figure 3C). To
189 exclude off-target effects we used different FBXO45 and MYCBP2 siRNAs to
190 reduce their expression in HeLa cells and confirmed that FBXW7α protein
191 levels were upregulated in cells that were FBXO45 or MYCBP2-depleted
192 under prolonged mitotic arrest (Figure EV3C). The effect could be confirmed
193 in U2OS cells using nocodazole and in HeLa cells using different inhibitors
194 that cause a mitotic arrest (Figures EV3D-I). We also aimed to confirm the
195 observed regulation of FBXW7α protein levels by expression of a dominant-
196 negative MYCBP2(1951-2950) fragment that binds FBXO45 and FBXW7α but
197 lacks the RING domain (Figures EV2A-B). Upon ectopical expression of Flag-
198 MYCBP2(1951-2950) we found that FBXW7α protein levels were specifically
199 upregulated in mitotic cells after treatment with nocodazole (Figure 3D).
200 Taken together, FBXO45 binds FBXW7α in mitotic cells and the FBXO45-
201 MYCBP2 complex regulates FBXW7α protein levels specifically during mitotic
202 arrest.
203
204

205 **FBXO45-MYCBP2 targets FBXW7α for ubiquitylation and degradation**
206 To find out whether the regulation of FBXW7α by FBXO45-MYCBP2 is
207 mediated by ubiquitylation we carried out *in vivo* ubiquitylation assays. We
208 found that both overexpression of FBXO45 and MYCBP2 promote
209 ubiquitylation of FBXW7α (Figure 4A). Deletion of the FBXO45 binding site in
210 FBXW7α reduced the ubiquitylation of FBXW7α markedly in *in vivo*
211 ubiquitylation assays using FBXW7αΔ106-126 expression (Figure 4B). To
212 study the effect of FBXO45 on FBXW7α protein stability, we depleted
213 FBXO45 in nocodazole-treated cells and added cycloheximide to block
214 translation. Cells were then harvested at different time points after
215 cycloheximide addition. In FBXO45-depleted cells FBXW7α was markedly
216 stabilized (Figure 4C) suggesting that FBXO45 promotes degradation of
217 FBXW7α upon mitotic arrest. In addition, Flag-FBXW7αΔ106-126 was
218 stabilized in comparison to full-length Flag-FBXW7α. The stability of Flag-
219 FBXW7α was increased by MG132 treatment (Figure 4D). From these
220 experiments, we conclude that FBXO45-MYCBP2 mediated degradation of
221 FBXW7α during prolonged mitosis depends on the proteasome.
222
223 **FBXO45-MYCBP2 reduces the sensitivity of cells to spindle poisons**
224 Previous studies have shown that FBXW7 regulates mitotic cell fate. In fact,
225 FBXW7 promotes mitotic cell death and prevents mitotic slippage in cells that
226 have been treated with anti-microtubule drugs to arrest them in mitosis [21]
227 [22], which is in line with its function as a tumor suppressor. As we had found
228 that FBXO45-MYCBP2 regulates FBXW7α protein levels during mitotic arrest
229 (Figure 3), we asked whether the FBXO45-MYCBP2 complex as a regulator
230 of FBXW7 would also affect mitotic cell fate. To test this, we analyzed mitotic
231 cell fate by live-cell imaging (Figure 5A, Video S1-2). For our live-cell imaging
232 analysis, we treated the cells with spindle poisons at concentrations that
233 completely prevented cell division and caused either mitotic cell death or
234 mitotic slippage [38]. As shown in Figure 5B, reduction of FBXO45 led to an
235 increase in mitotic cell death in cells that were arrested in mitosis with
236 nocodazole. Similar effects were observed in cells arrested in mitosis by Taxol
237 or vincristine treatment (Figures EV4A-B). To exclude off-target effects we
238 used siRNAs targeting different regions of FBXO45 mRNA (Figure 5B). In

239 addition, expression of an siRNA-resistant version of Flag-FBXO45 was able
240 to rescue the effect on mitotic cell fate (Figure 5C). Moreover, siRNA-
241 mediated downregulation of MYCBP2 also caused an increase in mitotic cell
242 death (Figure EV4C). In contrast, FBXO45 and MYCBP2 depletion did not
243 have an effect on progression of cells through an unperturbed mitosis (Figure
244 EV4D). To verify the results in an siRNA independent approach, we analyzed
245 the effect of the dominant-negative MYCBP2(1951-2950) fragment on mitotic
246 cell fate. As expected, overexpression of Flag-MYCBP2(1951-2950)
247 increased mitotic cell death (Figure 5D). Taken together, our results showed
248 that the FBXO45-MYCBP2 complex negatively regulates mitotic cell death
249 and increases mitotic slippage, suggesting that it has an opposing function
250 during mitotic arrest compared to FBXW7. This is in line with the FBXO45-
251 MYCBP2 complex being a negative regulator of FBXW7α during mitotic
252 arrest. We therefore asked whether the observed effect of FBXO45-MYCBP2
253 on mitotic cell fate depends on FBXW7. In fact, FBXW7 depletion was able to
254 rescue the effect of FBXO45, suggesting that FBXW7 is the downstream
255 target of the FBXO45-MYCBP2 complex that mediates mitotic cell fate
256 regulation (Figure 5E). Together, our data strongly suggest that FBXO45-
257 MYCBP2-mediated degradation of FBXW7 under prolonged mitotic arrest
258 induces mitotic slippage and prevents mitotic cell death.
259 Prolonged mitotic arrest is caused by a sustained activation of the spindle
260 assembly checkpoint (SAC). If the SAC cannot be satisfied and mitosis
261 cannot be completed, there are two alternative cell fates. Cells either undergo
262 mitotic cell death or perform mitotic slippage. Cell fate following mitotic arrest
263 is regulated by two competing networks, namely Cyclin B1 degradation and
264 pro-apoptotic caspase activation [39]. Besides cell fate regulation through
265 Cyclin B1, MCL-1, a pro-survival member of the BCL-2 family, was shown to
266 be involved in cell fate decision. MCL-1 is degraded by a ubiquitin-
267 proteasome-dependent mechanism in response to the disruption of mitosis,
268 resulting in cell death [39] [30] [22].
269 The tumor suppressor FBXW7 also plays important roles in mitotic cell fate
270 decision [22] [29] [21]. However, whether or not FBXW7 has a direct role in
271 regulating MCL-1 levels is a matter of debate [22] [40] [29] and therefore the

272 identification of the substrate(s) of FBXW7 involved in regulating mitotic cell
273 fate is an important task for future studies.
274 Our work identifies FBXO45 as a protein binding to a conserved acidic amino
275 acid motif (aa106-126) of FBXW7α (Figures 1-2) to form a ternary complex
276 with MYCBP2. Interestingly, available TCGA data show that FBXO45 is
277 frequently overexpressed in different cancer types (cBioPortal for Cancer
278 Genomics) [41] [42]. Therefore, it could be meaningful to further characterize
279 FBXO45 as a putative oncoprotein in future studies. MYCBP2 has been
280 recently uncovered as a novel type of E3 ligase with esterification activity
281 leading to ubiquitylation of serine and threonine residues in substrates [43],
282 which is intrinsic to higher eukaryotes. In the future, it would therefore be
283 interesting to see whether FBXW7 could be ubiquitylated on hydroxyl groups
284 by MYCBP2.
285 As FBXW7α is a nuclear protein but FBXO45 is found in the cytoplasm
286 (Figure 3A), the two proteins can only interact upon nuclear envelope
287 breakdown (Figure 3B). However, since mitosis is a relatively short process in
288 the eukaryotic cell cycle, the successful formation of a sustained interaction
289 between FBXO45 and FBXW7α as well as FBXW7α ubiquitylation may
290 require a longer arrest in mitosis. Interestingly, the degradation of two other
291 regulators of mitotic cell fate, MCL-1 and Cyclin B1, has also been shown to
292 occur in a slow and gradual manner during mitotic arrest [18] [30].
293 In the future, the development of a specific inhibitor to block the FBXO45-
294 MYCBP2-FBXW7α axis might actively promote mitotic cell death and prevent
295 mitotic slippage. Therefore, treatment of cancer patients with this inhibitor
296 after or in combination with anti-microtubule drugs could be a promising
297 approach in order to increase the efficiency of chemotherapeutic treatment.
298

299 **MATERIALS AND METHODS**

300

301 **Cell culture and transfection**

302 Human cell lines were grown in a humidified atmosphere with 5% CO_2 at
303 37°C. HeLa, U2OS and U2OS Flp-In-T-Rex cells were cultured in Dulbecco's
304 Modified Eagle's Medium (DMEM, Sigma-Aldrich) with 1 g/l glucose. HEK-
305 293T cells were grown in DMEM with 4.5 g/l glucose. The media were

306 supplemented with 10% fetal bovine serum (FBS, Sigma-Aldrich or Thermo
307 Scientific). HeLa GFP-α-tubulin/RFP-H2B cells (D. Gerlich, ETH Zürich) were
308 cultured in DMEM containing 1 g/l glucose, 10% FBS, 500 µg/ml G418 and
309 0.5 µg/ml puromycin. The T-Rex system was used to generate U2OS Flp-In-
310 T-Rex Flag-FBXW7α, U2OS Flp-In-T-Rex Flag-FBXW7αΔ106-126 and U2OS
311 Flp-In-T-Rex Flag-MYCBP2(1951-2950) stable cell lines according to the
312 manufacturer's instructions (Life Technologies).
313 Cell culture work was performed under sterile conditions. Cell line
314 authentication was regularly performed by Multiplexion in Heidelberg.
315 HEK-293T and HeLa cells were transiently transfected with plasmid DNA
316 using polyethylenimine (PEI, Polysciences) at a final concentration of 5 µg/ml.
317 The cells were incubated at 37°C and harvested 24-48 h after transfection. If
318 the cells were harvested 48 h after transfection, the transfection mixture was
319 removed 6-24 h after transfection and replaced by fresh growth medium.
320 For the transfection of HeLa or U2OS cells with siRNA, the transfection
321 reagent Lipofectamine 2000 (Invitrogen) was used according to the
322 manufacturer's instructions. Cells were transfected with 30 nM of siRNA for
323 72 h. For rescue experiments, 50 ng of plasmid were co-transfected with
324 40 nM of siRNA for 72 h.
325 The following siRNA sequences were used:
326 GL2 (firefly luciferase, control), 5'-CGUACGCGGAAUACUUCGAtt-3';
327 FBXO45 #1, 5'-GGAGAAAGAAUUCGAGUCAtt-3';
328 FBXO45 #2, 5'-ACACAUGGUUAUUGCGUAUtt-3';
329 FBXW7, 5'-ACAGGACAGUGUUUACAAAtt-3';
330 MYCBP2 #1, 5'-CCCGAGAUCUUGGGAAUAAtt-3'.
331 FBXO45 #3 (200933, L-023542-01-0005) and MYCBP2 #2 (23077, L-006951-
332 00-0005) were purchased as SMARTpools from Dharmacon. If not stated
333 otherwise, FBXO45 siRNA #2 was used for FBXO45 depletion and MYCBP2
334 siRNA #2 was transfected in order to downregulate MYCBP2.
335
336 **Cell cycle synchronization**
337 In order to arrest HeLa or U2OS cells in G1/S phase, the cells were treated
338 with 2 mM thymidine for 18 h. In order to arrest HeLa or U2OS cells in mitosis,
339 cells were first synchronized in G1/S phase by treatment with 2 mM thymidine

340 for 17 h. The cells were released into the cell cycle by washing three times
341 with PBS and incubation with fresh growth medium for 5 h. Finally, the cells
342 were treated with 250 ng/ml nocodazole, 500-1000 nM Taxol, 500 nM
343 vincristine, 5 µM STLC or 100 nM BI2536 for 16-17 h. Mitotic cells were
344 collected by a mitotic shake-off.
345
346 **MG132 and cycloheximide treatment**
347 In order to inhibit proteasomal degradation in HEK-293T cells, the cells were
348 treated with 10 µM MG132 (Sigma-Aldrich) for 4-5 h before harvesting. In
349 order to inhibit protein synthesis in HeLa cells, they were treated with
350 100 µg/ml cycloheximide (Sigma-Aldrich). For a cycloheximide chase assay,
351 the cells were harvested at different time points after cycloheximide treatment.
352
353 **Live-cell imaging**
354 For the analysis of mitotic cell fate or unperturbed mitotic progression, live-cell
355 imaging was performed. For mitotic cell fate analysis, U2OS cells were
356 transfected with 30 nM siRNA targeting GL2, FBXW7, FBXO45 or MYCBP2.
357 48 h after transfection, 2.5 x 10^4 cells were seeded into Ibidi dish chambers.
358 72 h after transfection, the cells were treated with 250 ng/ml nocodazole,
359 1 µM Taxol or 500 nM vincristine. 4 h after the spindle poison treatment, the
360 cells were monitored by a 10x/0.3 EC PlnN Ph1 DICI objective on a Zeiss Cell
361 Observer Z1 inverted microscope (AxioCam MRm camera system) with
362 incubation at 5% CO_2 and 37°C. Multi-tile phase-contrast images were taken
363 every 10 min for 48 h using the Zeiss ZEN blue software. Data analysis was
364 performed with ImageJ Fiji software. Cell death was defined by cell
365 morphology and cessation of movement. Mitotic slippage was defined by
366 mitotic exit without cell division. For the analysis of unperturbed mitotic
367 progression, HeLa GFP-α-tubulin/RFP-H2B cells were transfected with 30 nM
368 siRNA targeting GL2 or FBXO45 and MYCBP2. Analysis was performed as
369 described previously [44]. 48 h after transfection, 2.5 x 10^4 cells were seeded
370 into Ibidi dish chambers and arrested in G1/S phase by thymidine treatment.
371 24 h after thymidine addition, the cells were released from the arrest and
372 analyzed by live-cell imaging using LED module Colibri.2 with 470 nm for GFP
373 and 590 nm for RFP fluorochrome excitation.

374

375 **Preparation of protein extracts from mammalian cells**

376 For the preparation of cell extracts, cell pellets were resuspended in 3-5
377 volumes of RIPA, NP40 or Urea lysis buffer. RIPA lysis buffer (50 mM Tris-
378 HCl pH 7.4, 1% NP40, 0.5% Na-deoxycholate, 0.1% SDS, 150 mM NaCl,
379 2 mM EDTA, 50 mM NaF, 1 mM DTT, 10 µg/ml TPCK, 5 µg/ml TLCK, 0.1 mM
380 Na_3VO_4, 1 µg/ml Aprotinin, 1 µg/ml Leupeptin, 10 µg/ml Trypsin inhibitor from
381 soybean) was used for the analysis of protein levels in whole cell extracts and
382 for *in vivo* ubiquitylation assays. NP40 lysis buffer (40 mM Tris-HCl pH 7.5,
383 150 mM NaCl, 5 mM EDTA, 10 mM β-glycerophosphate, 5 mM NaF, 0.5%
384 NP40, 1 mM DTT, 10 µg/ml TPCK, 5 µg/ml TLCK, 0.1 mM Na_3VO_4, 1 µg/ml
385 Aprotinin, 1 µg/ml Leupeptin, 10 µg/ml Trypsin inhibitor from soybean) was
386 used for immunoprecipitations. Urea lysis buffer (8 M Urea, 30 mM imidazole,
387 0.1 M phosphate buffer pH 8.0) was used for *in vivo* ubiquitylation assays.
388 The cell lysates were incubated on ice for 30 min with short vortexing every 5-
389 10 min. The lysates were cleared by centrifugation at maximal speed and 4°C
390 in an Eppendorf 5415 R centrifuge for 15 min. The supernatants were
391 transferred to fresh reaction tubes. Extracts of cytoplasmic and nuclear cell
392 fractions were prepared using the CelLytic NuCLEAR Extraction Kit (Sigma)
393 according to the manufacturer's instructions.
394 The protein concentration of a cell extract was determined according to the
395 Bradford method in a Bio-Rad Protein assay. For SDS-PAGE, the cell extracts
396 were mixed with equal volumes of 2x Laemmli buffer and incubated at 95°C
397 for 5 min.

398

399 **Western blotting**

400 The following antibodies were used for Western blotting: Rabbit α-FBXW7α
401 antibody (A301-720A, 1:15000) was obtained from Bethyl. Rabbit α-FBXO45
402 (NBP1-91891, 1:500) was purchased from Novus. Rabbit α-MYCBP2 was a
403 kind gift from K. Scholich [45]. Mouse α-Flag (M2, F3165, 1:5000), mouse α-
404 tubulin (B-5-1-2, 1:10000) and mouse α-Vinculin (hVIN-1, 1:5000) were
405 obtained from Sigma-Aldrich. Rabbit α-Cyclin B1 has been described before
406 [46]. Mouse α-HA (16B12, 1:1000) was purchased from Babco. Mouse α-Myc
407 (9E10, 1:500), rabbit α-SKP1 (H-163, 1:1000) and mouse α-ubiquitin (P4D1,

408 1:1000) were obtained from Santa Cruz. Mouse α-Nucleophosmin (NPM, 32-
409 5200, 1:1000) was ordered from Zymed. Rabbit α-MCL-1 (4572, 1:1000) was
410 obtained from Cell Signaling. Goat α-mouse IgG HRP (1:5000) was
411 purchased from Novus. Donkey α-rabbit IgG HRP (1:5000) was obtained from
412 Jackson Laboratories.
413
414 **Immunoprecipitation**
415 Immunoprecipitations of Flag-tagged proteins were performed using α-Flag
416 M2 affinity beads (Sigma-Aldrich). For each immunoprecipitation reaction, 10-
417 40 µl of the α-Flag M2 affinity bead suspension was used. The beads were
418 washed twice with TBS, once with glycine buffer (0.1 M glycine-HCl pH 3.5)
419 and three times with TBS. Buffers and beads were kept on ice and
420 centrifugations were performed at 5000 rpm and 4°C for 2 min in an
421 Eppendorf 5415 R centrifuge. HEK-293T or HeLa cell extracts were prepared
422 with NP40 lysis buffer and 6-15 mg of each extract were transferred to the
423 prepared beads. Each reaction was filled up to a final volume of 1 ml using
424 NP40 lysis buffer. The reactions were incubated overnight on a rotating wheel
425 at 4°C. After the incubation, the beads were washed 3-5 times with NP40 lysis
426 buffer. Immunoprecipitated proteins were eluted from the beads by
427 competition with 100 µl of a 3x Flag peptide solution (100-500 ng/µl in NP40
428 lysis buffer). The elution was carried out on ice for 30 min with short vortexing
429 every 5-10 min. After the elution, the beads were centrifuged at 5000 rpm and
430 4°C for 2 min. 90 µl of the supernatant were transferred to a fresh reaction
431 tube and 30 µl of 4x Laemmli buffer were added. After incubation at 95°C for
432 2 min, 20-40% of the immunoprecipitation sample were analyzed by SDS-
433 PAGE and Western blotting.
434 In order to analyze whether proteins exist in ternary complexes, sequential
435 immunoprecipitations were performed. In the first step of the experiment, 15-
436 20 mg of HEK-293T cell extracts were used for an immunoprecipitation
437 directed against a Flag-tagged MYCBP2 fragment. The immunoprecipitation
438 was performed as described above. Instead of mixing the eluate with Laemmli
439 buffer, it was used for a second immunoprecipitation directed against HA-
440 FBXO45. HA-FBXO45 was immunoprecipitated with 20 µl of α-HA agarose
441 beads (Sigma-Aldrich) according to the manufacturer's instructions. Finally,

442 the beads were incubated with 30 µl of 2x Laemmli buffer at 95°C for 5 min.
443 The supernatant was analyzed by SDS-PAGE and Western blotting.
444
445 **Mass spectrometry analysis**
446 Immunoprecipitation samples were analyzed by SDS-PAGE and stained by
447 Colloidal Coomassie. Analysis was performed by M. Schnölzer (DKFZ Protein
448 Analysis Facility, Heidelberg). Briefly, whole gel lanes were cut into slices.
449 Proteins were reduced and alkylated by incubation with 10 mM DTT in 40 mM
450 NH_4HCO_3 for 1 h at 56°C in the dark and incubation with 55 mM
451 iodoacetamide in 40 mM NH_4HCO_3 for 30 min at 25°C. After washing of the
452 slices with H_2O and 50% acetonitrile, they were dried with 100% acetonitrile.
453 Proteins were digested in-gel with trypsin (0.17 µg in 10 µl 40 mM NH_4HCO_3,
454 Promega) at 37°C over night. Tryptic peptides were extracted with 50%
455 acetonitrile/0.1% TFA and 100% acetonitrile. Supernatants were lyophilized
456 and redissolved in 0.1% TFA/5% hexafluoroisopropanol. Solutions were
457 analyzed by nanoLC-ESI-MS/MS. Peptides were separated with a
458 nanoAcquity UPLC system (Waters GmbH). Peptides were loaded on a C18
459 trap column with a particle size of 5 µm (Waters GmbH). Liquid
460 chromatography was carried out on a BEH130 C18 column with a particle size
461 of 1.7 µm (Waters GmbH). A 1 h gradient was applied for protein
462 identification. The nanoUPLC system was connected to an LTQ Orbitrap XL
463 mass spectrometer (Thermo Scientific). Data were acquired with the Xcalibur
464 software 2.1 (Thermo Scientific). The SwissProt database (taxonomy human)
465 was used for database searches with the MASCOT search engine (Matrix
466 Science). Data from individual gel slices were merged. Peptide mass
467 tolerance was 5 ppm, fragment mass tolerance was 0.4 Da and significance
468 threshold was $p<0.01$.
469
470 ***In vivo* ubiquitylation assays**
471 HEK-293T cells transiently transfected with the indicated plasmids were
472 treated with 10 µM MG132 4-5 h before harvesting. Cells were harvested and
473 cell extracts were prepared with RIPA lysis buffer containing 10 mM of the
474 DUB inhibitor N-ethylmaleimide (NEM). 2-3 mg of protein extract were used
475 for each sample. Flag-FBXW7α was immunoprecipitated with α-Flag affinity

476 beads. Immunoprecipitation and washing steps were performed with RIPA
477 lysis buffer containing 10 mM NEM. Alternatively, endogenous FBXW7α was
478 immunoprecipitated by incubation of each protein extract with 1 µg of
479 FBXW7α antibody on a rotating wheel at 4°C overnight. After the incubation
480 with the antibody, the extracts were incubated with 15 µl of protein A
481 sepharose beads (GE Healthcare) on a rotating wheel at 4°C for 1 h. The
482 beads were washed four times with RIPA lysis buffer containing 10 mM NEM.
483 Finally, the beads were incubated in 30 µl of 2x Laemmli buffer at 95°C for
484 5 min. 25 µl of the supernatant were analyzed by SDS-PAGE and Western
485 blotting.
486 For denaturing ubiquitylation assays, cell extracts were prepared using Urea
487 lysis buffer. Cell extracts were sonified, centrifuged and incubated with Nickel-
488 NTA agarose beads on a rotating wheel at RT for 2 h. Afterwards, the beads
489 were washed four times with Urea lysis buffer and proteins were finally eluted
490 using 30 µl of 2x Laemmli buffer containing 200 mM imidazole. 25 µl of the
491 supernatant were analyzed by SDS-PAGE and Western blotting.
492
493 **Expression and purification of MBP-tagged proteins**
494 Chemically competent *E. coli* Rosetta (DE3) were transformed with pMAL-
495 MBP-FBXW7α-N167. A single colony was used to inoculate 10 ml of LB
496 medium containing 100 µg/ml ampicillin and 0.2% glucose. The culture was
497 incubated over night at 30°C with constant shaking at 180 rpm. The overnight
498 culture was used to inoculate 1 l of LB medium containing 100 µg/ml
499 ampicillin and 0.2% glucose. The culture was incubated at 37°C with constant
500 shaking at 180 rpm. When an OD_{600} of 0.5 was reached, the culture was
501 cooled down on ice at 4°C and protein expression was induced by the
502 addition of 0.4 mM isopropyl-β-D-thiogalactopyranoside (IPTG). The culture
503 was further incubated over night at 18°C with constant shaking at 180 rpm.
504 Bacteria were harvested by centrifugation at 5000 rpm and 4°C for 15 min
505 (F10-6x500Y rotor, Piramoon). The pellet was resuspended in 25 ml of cold
506 column buffer. Cell lysis was performed with a high pressure homogenizer
507 (15000-17000 psi/1030-1170 bar for one pass, EmulsiFlex C5, Avestin). The
508 lysate was centrifuged at 20000 g and 4°C for 20 min (WX Ultra 80, Thermo
509 Scientific). The supernatant was applied onto a column with 1 ml of

510 equilibrated amylose resin (NEB). The column with the beads and the extract
511 was incubated on a rotating wheel at 4°C for 1 h. Afterwards, the beads were
512 washed three times with 15 ml of column buffer. Finally, the proteins bound to
513 the beads were eluted with 5 ml of column buffer containing 10 mM maltose.
514 10 fractions of 500 µl each were collected. Protein containing fractions were
515 identified by spotting the fractions on nitrocellulose and staining with Ponceau
516 S solution. Protein containing fractions were pooled and MBP-FBXW7α-N167
517 was further purified with a preparative Superdex 200 column in 50 mM Tris-
518 HCl pH 8.0, 100 mM NaCl, 5 mM β-mercaptoethanol, 5% glycerol. Purified
519 MBP-FBXW7α-N167 fractions were analyzed by SDS-PAGE and Colloidal
520 Coomassie staining. Protein containing fractions were aliquoted, frozen in
521 liquid nitrogen and stored at -80°C.
522
523 ***In vitro* transcription and translation and *in vitro* binding assays**
524 For *in vitro* binding assays, FBXO45 and MYCBP2(1951-2950) cDNA
525 sequences in pCMV-3Tag1A backbones were transcribed and translated *in*
526 *vitro* using the TNT T3 coupled reticulocyte system (Promega) according to
527 the manufacturer's instructions. The proteins were synthesized in the
528 presence of 20 µCi [^{35}S]-methionine so that synthesized proteins were
529 radioactively labelled. 20 µl of the *in vitro* translated proteins were incubated
530 with 10 µg of MBP-FBXW7α-N167 or MBP alone coupled to 10 µl of amylose
531 beads in a final volume of 500 µl NP40 lysis buffer on a rotating wheel at 4°C
532 for 2 h. The beads were washed five times with 800 µl of NP40 lysis buffer.
533 Finally, the beads were incubated with 30 µl of 2x Laemmli buffer at 95°C for
534 5 min. Input and pull-down samples were analyzed by SDS-PAGE and
535 stained with Colloidal Coomassie. The gel was then incubated with
536 Amersham Amplify Fluorographic reagent (GE Healthcare) for 30 min with
537 gentle shaking. Afterwards, the gel was dried at 80°C for 1 h in a vacuum
538 dryer and analyzed by autoradiography.
539
540 **FACS analysis**
541 For the analysis of mitotic arrest, the cellular DNA content was measured by
542 FACS analysis. Cells were fixed with 70% ethanol at -20 °C and rehydrated in
543 PBS for 15 min at RT. Afterwards, the cells were resuspended in 300 µl of PI

544 staining solution (30 µg/ml propidium iodide, 10 µg/ml RNase A in PBS) and
545 incubated for 15 min at RT. Stained cells were analyzed on a FACSCalibur
546 (BD).
547
548 **ACKNOWLEDGMENTS**
549
550 We thank D. Gerlich, L. Hengst, F. Melchior, G. Melino, A. Peschiaroli and K.
551 Scholich for providing reagents and cell lines. We acknowledge the DKFZ
552 Mass Spectrometry and Microscopy Core Facilities for providing equipment
553 and excellent technical assistance. We thank Bettina Dörr for expert technical
554 assistance. We acknowledge the members of our lab for critically reading the
555 manuscript. This work was supported by a grant from the German Cancer Aid
556 (Deutsche Krebshilfe) No. 110924 to I.Hoffmann.
557
558 **AUTHOR CONTRIBUTION**
559 IH and KTR designed the experiments. KTR, YTK and BV performed the
560 experiments. IH and KTR wrote the paper.
561
562 **DECLARATION OF INTERESTS**
563 The authors declare no conflict of interests.
564
565 **REFERENCES**
566 1. Hershko A, Ciechanover A (1998) The ubiquitin system. *Annual review*
567 *of biochemistry* **67**: 425-79
568 2. Davis RJ, Welcker M, Clurman BE (2014) Tumor suppression by the
569 Fbw7 ubiquitin ligase: mechanisms and opportunities. *Cancer cell* **26**: 455-64
570 3. Nateri AS, Riera-Sans L, Da Costa C, Behrens A (2004) The ubiquitin
571 ligase SCFFbw7 antagonizes apoptotic JNK signaling. *Science* **303**: 1374-8
572 4. Wei W, Jin J, Schlisio S, Harper JW, Kaelin WG, Jr. (2005) The v-Jun
573 point mutation allows c-Jun to escape GSK3-dependent recognition and
574 destruction by the Fbw7 ubiquitin ligase. *Cancer cell* **8**: 25-33
575 5. Welcker M, Orian A, Jin J, Grim JE, Harper JW, Eisenman RN,
576 Clurman BE (2004) The Fbw7 tumor suppressor regulates glycogen synthase
577 kinase 3 phosphorylation-dependent c-Myc protein degradation. *Proceedings*
578 *of the National Academy of Sciences of the United States of America* **101**:
579 9085-90
580 6. Yada M, Hatakeyama S, Kamura T, Nishiyama M, Tsunematsu R,
581 Imaki H, Ishida N, Okumura F, Nakayama K, Nakayama KI (2004)

582 Phosphorylation-dependent degradation of c-Myc is mediated by the F-box
583 protein Fbw7. *The EMBO journal* **23**: 2116-25
584 7. Koepp DM, Schaefer LK, Ye X, Keyomarsi K, Chu C, Harper JW,
585 Elledge SJ (2001) Phosphorylation-dependent ubiquitination of cyclin E by the
586 SCFFbw7 ubiquitin ligase. *Science* **294**: 173-7
587 8. Moberg KH, Bell DW, Wahrer DC, Haber DA, Hariharan IK (2001)
588 Archipelago regulates Cyclin E levels in Drosophila and is mutated in human
589 cancer cell lines. *Nature* **413**: 311-6
590 9. Strohmaier H, Spruck CH, Kaiser P, Won KA, Sangfelt O, Reed SI
591 (2001) Human F-box protein hCdc4 targets cyclin E for proteolysis and is
592 mutated in a breast cancer cell line. *Nature* **413**: 316-22
593 10. Hubbard EJ, Wu G, Kitajewski J, Greenwald I (1997) sel-10, a negative
594 regulator of lin-12 activity in Caenorhabditis elegans, encodes a member of
595 the CDC4 family of proteins. *Genes & development* **11**: 3182-93
596 11. Gupta-Rossi N, Le Bail O, Gonen H, Brou C, Logeat F, Six E,
597 Ciechanover A, Israel A (2001) Functional interaction between SEL-10, an F-
598 box protein, and the nuclear form of activated Notch1 receptor. *The Journal of*
599 *biological chemistry* **276**: 34371-8
600 12. Galan JM, Peter M (1999) Ubiquitin-dependent degradation of multiple
601 F-box proteins by an autocatalytic mechanism. *Proceedings of the National*
602 *Academy of Sciences of the United States of America* **96**: 9124-9
603 13. Duda DM, Olszewski JL, Tron AE, Hammel M, Lambert LJ, Waddell
604 MB, Mittag T, DeCaprio JA, Schulman BA (2012) Structure of a glomulin-
605 RBX1-CUL1 complex: inhibition of a RING E3 ligase through masking of its
606 E2-binding surface. *Molecular cell* **47**: 371-82
607 14. Tron AE, Arai T, Duda DM, Kuwabara H, Olszewski JL, Fujiwara Y,
608 Bahamon BN, Signoretti S, Schulman BA, DeCaprio JA (2012) The
609 glomuvenous malformation protein Glomulin binds Rbx1 and regulates cullin
610 RING ligase-mediated turnover of Fbw7. *Molecular cell* **46**: 67-78
611 15. Ekholm-Reed S, Goldberg MS, Schlossmacher MG, Reed SI (2013)
612 Parkin-dependent degradation of the F-box protein Fbw7beta promotes
613 neuronal survival in response to oxidative stress by stabilizing Mcl-1.
614 *Molecular and cellular biology* **33**: 3627-43
615 16. Cizmecioglu O, Krause A, Bahtz R, Ehret L, Malek N, Hoffmann I
616 (2012) Plk2 regulates centriole duplication through phosphorylation-mediated
617 degradation of Fbxw7 (human Cdc4). *Journal of cell science* **125**: 981-92
618 17. Rieder CL, Maiato H (2004) Stuck in division or passing through: what
619 happens when cells cannot satisfy the spindle assembly checkpoint.
620 *Developmental cell* **7**: 637-51
621 18. Brito DA, Rieder CL (2006) Mitotic checkpoint slippage in humans
622 occurs via cyclin B destruction in the presence of an active checkpoint. *Curr*
623 *Biol* **16**: 1194-200
624 19. Frederiks CN, Lam SW, Guchelaar HJ, Boven E (2015) Genetic
625 polymorphisms and paclitaxel- or docetaxel-induced toxicities: A systematic
626 review. *Cancer Treat Rev* **41**: 935-50
627 20. Haschka M, Karbon G, Fava LL, Villunger A (2018) Perturbing mitosis
628 for anti-cancer therapy: is cell death the only answer? *EMBO Rep* **19**
629 21. Finkin S, Aylon Y, Anzi S, Oren M, Shaulian E (2008) Fbw7 regulates
630 the activity of endoreduplication mediators and the p53 pathway to prevent
631 drug-induced polyploidy. *Oncogene* **27**: 4411-21

632 22. Wertz IE, Kusam S, Lam C, Okamoto T, Sandoval W, Anderson DJ,
633 Helgason E, Ernst JA, Eby M, Liu J*, et al.* (2011) Sensitivity to antitubulin
634 chemotherapeutics is regulated by MCL1 and FBW7. *Nature* **471**: 110-4
635 23. Grill B, Murphey RK, Borgen MA (2016) The PHR proteins: intracellular
636 signaling hubs in neuronal development and axon degeneration. *Neural Dev*
637 **11**: 8
638 24. Po MD, Hwang C, Zhen M (2010) PHRs: bridging axon guidance,
639 outgrowth and synapse development. *Curr Opin Neurobiol* **20**: 100-7
640 25. Chen X, Sahasrabuddhe AA, Szankasi P, Chung F, Basrur V,
641 Rangnekar VM, Pagano M, Lim MS, Elenitoba-Johnson KS (2014) Fbxo45-
642 mediated degradation of the tumor-suppressor Par-4 regulates cancer cell
643 survival. *Cell Death Differ* **21**: 1535-45
644 26. Kugler JM, Woo JS, Oh BH, Lasko P (2010) Regulation of Drosophila
645 vasa in vivo through paralogous cullin-RING E3 ligase specificity receptors.
646 *Molecular and cellular biology* **30**: 1769-82
647 27. Nakata K, Abrams B, Grill B, Goncharov A, Huang X, Chisholm AD, Jin
648 Y (2005) Regulation of a DLK-1 and p38 MAP kinase pathway by the ubiquitin
649 ligase RPM-1 is required for presynaptic development. *Cell* **120**: 407-20
650 28. Xiong X, Hao Y, Sun K, Li J, Li X, Mishra B, Soppina P, Wu C, Hume
651 RI, Collins CA (2012) The Highwire ubiquitin ligase promotes axonal
652 degeneration by tuning levels of Nmnat protein. *PLoS Biol* **10**: e1001440
653 29. Allan LA, Skowyra A, Rogers KI, Zeller D, Clarke PR (2018) Atypical
654 APC/C-dependent degradation of Mcl-1 provides an apoptotic timer during
655 mitotic arrest. *The EMBO journal* **37**
656 30. Harley ME, Allan LA, Sanderson HS, Clarke PR (2010)
657 Phosphorylation of Mcl-1 by CDK1-cyclin B1 initiates its Cdc20-dependent
658 destruction during mitotic arrest. *The EMBO journal* **29**: 2407-20
659 31. Kourtis N, Moubarak RS, Aranda-Orgilles B, Lui K, Aydin IT, Trimarchi
660 T, Darvishian F, Salvaggio C, Zhong J, Bhatt K*, et al.* (2015) FBXW7
661 modulates cellular stress response and metastatic potential through HSF1
662 post-translational modification. *Nature cell biology* **17**: 322-332
663 32. Huttlin EL, Bruckner RJ, Paulo JA, Cannon JR, Ting L, Baltier K, Colby
664 G, Gebreab F, Gygi MP, Parzen H*, et al.* (2017) Architecture of the human
665 interactome defines protein communities and disease networks. *Nature* **545**:
666 505-509
667 33. Liao EH, Hung W, Abrams B, Zhen M (2004) An SCF-like ubiquitin
668 ligase complex that controls presynaptic differentiation. *Nature* **430**: 345-50
669 34. Welcker M, Clurman BE (2008) FBW7 ubiquitin ligase: a tumour
670 suppressor at the crossroads of cell division, growth and differentiation.
671 *Nature reviews Cancer* **8**: 83-93
672 35. Skaar JR, Pagan JK, Pagano M (2013) Mechanisms and function of
673 substrate recruitment by F-box proteins. *Nature reviews Molecular cell biology*
674 **14**: 369-81
675 36. Kimura T, Gotoh M, Nakamura Y, Arakawa H (2003) hCDC4b, a
676 regulator of cyclin E, as a direct transcriptional target of p53. *Cancer Sci* **94**:
677 431-6
678 37. Pierre SC, Hausler J, Birod K, Geisslinger G, Scholich K (2004) PAM
679 mediates sustained inhibition of cAMP signaling by sphingosine-1-phosphate.
680 *The EMBO journal* **23**: 3031-40

681 38. Brito DA, Yang Z, Rieder CL (2008) Microtubules do not promote
682 mitotic slippage when the spindle assembly checkpoint cannot be satisfied.
683 *The Journal of cell biology* **182**: 623-9
684 39. Gascoigne KE, Taylor SS (2008) Cancer cells display profound intra-
685 and interline variation following prolonged exposure to antimitotic drugs.
686 *Cancer cell* **14**: 111-22
687 40. Sloss O, Topham C, Diez M, Taylor S (2016) Mcl-1 dynamics influence
688 mitotic slippage and death in mitosis. *Oncotarget* **7**: 5176-92
689 41. Cerami E, Gao J, Dogrusoz U, Gross BE, Sumer SO, Aksoy BA,
690 Jacobsen A, Byrne CJ, Heuer ML, Larsson E*, et al.* (2012) The cBio cancer
691 genomics portal: an open platform for exploring multidimensional cancer
692 genomics data. *Cancer Discov* **2**: 401-4
693 42. Gao J, Aksoy BA, Dogrusoz U, Dresdner G, Gross B, Sumer SO, Sun
694 Y, Jacobsen A, Sinha R, Larsson E*, et al.* (2013) Integrative analysis of
695 complex cancer genomics and clinical profiles using the cBioPortal. *Sci Signal*
696 **6**: pl1
697 43. Pao KC, Wood NT, Knebel A, Rafie K, Stanley M, Mabbitt PD,
698 Sundaramoorthy R, Hofmann K, van Aalten DMF, Virdee S (2018) Activity-
699 based E3 ligase profiling uncovers an E3 ligase with esterification activity.
700 *Nature* **556**: 381-385
701 44. Kratz AS, Richter KT, Schlosser YT, Schmitt M, Shumilov A, Delecluse
702 HJ, Hoffmann I (2016) Fbxo28 promotes mitotic progression and regulates
703 topoisomerase IIalpha-dependent DNA decatenation. *Cell Cycle* **15**: 3419-
704 3431
705 45. Dorr A, Pierre S, Zhang DD, Henke M, Holland S, Scholich K (2015)
706 MYCBP2 Is a Guanosine Exchange Factor for Ran Protein and Determines
707 Its Localization in Neurons of Dorsal Root Ganglia. *The Journal of biological*
708 *chemistry* **290**: 25620-35
709 46. Hoffmann I, Draetta G, Karsenti E (1994) Activation of the phosphatase
710 activity of human cdc25A by a cdk2-cyclin E dependent phosphorylation at the
711 G1/S transition. *The EMBO journal* **13**: 4302-10
712

713

714 **Figure 1. FBXW7 protein levels are reduced under prolonged mitotic**
715 **arrest**

716 (A) FBXW7α protein levels decrease during prolonged mitotic arrest. HeLa
717 cells were treated with 250 ng/ml nocodazole for 2 h. Mitotic cells were
718 collected by mitotic shake-off (time point 0) and further incubated with
719 250 ng/ml nocodazole. The cells were harvested at different time points by a
720 mitotic shake-off. (Top) Cell extracts were prepared and analyzed by Western
721 blotting. (Bottom, left) Relative FBXW7α signal intensities were quantified.
722 Average signal intensities and standard deviations from n=4 experiments
723 were calculated. Statistical significance (difference to time point 0) was
724 analyzed by a two-tailed, unpaired t-test with unequal variance. * $p<0.05$; **

725 p<0.01. (Bottom, right) Mitotic arrest was confirmed for two time points (0 h
726 and 8 h) by FACS analysis. Asynchronous (asy.) cells served as a control.
727 (B) Decrease in FBXW7α protein levels during prolonged mitotic arrest
728 depends on proteasomal activity. HeLa cells were treated with 250 ng/ml
729 nocodazole for 2 h. Mitotic cells were collected by mitotic shake-off (time point
730 0) and further incubated with 250 ng/ml nocodazole. MG132 was added in
731 order to inhibit the proteasome. Cells were harvested at different time points
732 by a mitotic shake-off. Cell extracts were prepared and analyzed by Western
733 blotting. Relative FBXW7α, Cyclin B1 and MCL-1 signal intensities were
734 quantified.
735 (C) Network of known and putative FBXW7 interaction partners.
736 Immunoprecipitation of Flag-FBXW7α from HEK-293T cells treated with the
737 proteasomal inhibitor MG132 for 4 h and subsequent mass spectrometry
738 analysis identified several known SCF components and the SCF regulators
739 NEDD8 and ARIH1 as well as FBXW7 substrates. Moreover, FBXO45 and
740 MYCBP2 were identified as FBXW7 interaction partners and could act as
741 putative FBXW7 regulators.
742
743 **Figure 2. FBXO45-MYCBP2 binds to a conserved N-terminal motif of**
744 **FBXW7α**
745 (A-B) FBXO45 and FBXW7α specifically interact in reciprocal
746 immunoprecipitations. Several Flag tagged F-box and DCAF proteins were
747 overexpressed in HEK-293T cells for 24 h. Cell extracts were used for an
748 immunoprecipitation directed against the Flag tag.
749 (C) (Top) Schematic representation of Δ106-126 deletion in FBXW7α used in
750 immunoprecipitation experiments. Positions of N-terminal domain (blue),
751 dimerization domain (green), F-box domain (yellow) and WD40 domain (red)
752 are indicated. (Bottom) FBXO45 and MYCBP2 interact with the N-terminal
753 domain of FBXW7α. Flag-FBXW7α FL or Flag-FBXW7αΔ106-126 were
754 overexpressed in HEK-293T cells for 24 h. Cell extracts were used for α-Flag
755 immunoprecipitations.
756 (D) Sequence alignment of amino acid residues 106-126 from human
757 FBXW7α with homologues from *Macaca mulatta, Mus musculus, Xenopus*
758 *laevis* and *Danio rerio*.

759 (E) Either MBP alone or MBP-FBXW7α-N167 were incubated with *in vitro*
760 translated and [^{35}S]-methionine containing FBXO45 or MYCBP2(1951-2950).
761 MBP was pulled down with amylose beads. Pull-down samples were analyzed
762 by SDS-PAGE and Colloidal Coomassie staining. *In vitro* translated proteins
763 were detected by autoradiography.
764 (F) FBXW7α forms a complex with MYCBP2 and FBXO45. Flag-
765 MYCBP2(1951-2950) and HA-FBXO45 were co-expressed in HEK-293T cells
766 for 24 h. Cell extracts were used for an immunoprecipitation with α-Flag
767 agarose beads. Immunoprecipitated proteins were eluted by competition with
768 Flag peptide. Eluates were used for a second immunoprecipitation directed
769 against the HA tag. Immunoprecipitates obtained after sequential
770 immunoprecipitation were analyzed by Western blotting.
771
772 **Figure 3. FBXO45 and MYCBP2 downregulate FBXW7α protein levels**
773 **during mitotic arrest**
774 (A) FBXW7α is a nuclear protein, whereas FBXO45 is localized in the
775 cytoplasm. Cytoplasmic and nuclear extracts were prepared from HeLa cells
776 and analyzed by Western blotting.
777 (B) FBXO45 and FBXW7α interact predominantly in mitosis. Flag-FBXO45
778 was overexpressed in HeLa cells. Asynchronous or mitotic cells that had been
779 treated with nocodazole for 17 h were harvested. Cytoplasmic extracts were
780 used for an immunoprecipitation directed against the Flag tag.
781 (C) HeLa cells were transfected with 30 nM FBXO45 or FBXW7 siRNAs for
782 72 h. GL2 siRNA was used as a control. The cells were arrested in mitosis by
783 nocodazole (noco.) treatment for 17 h and collected by a mitotic shake-off.
784 Mitotic cells were compared with an asynchronous (asy.) cell population.
785 (Top) Cell extracts were analyzed by Western blotting. Crossreacting band in
786 FBXO45 immunoblot is marked with an asterisk. As the samples were
787 analyzed in three Western blots, three vinculin immunoblots are shown as
788 loading controls. (Bottom) Quantification of relative FBXW7α and FBXO45
789 signal intensities are shown. Relative FBXW7α and FBXO45 signals in the
790 GL2 controls were set to 1. Average signal intensities and standard deviations
791 from n=4 experiments were calculated. Statistical significance was analyzed

792 by a two-tailed, unpaired t-test with unequal variance. * $p<0.05$; n.s.: not
793 significant.
794 (D) Expression of Flag-MYCBP2(1951-2950) was induced in a stable U2OS
795 Flp-In-T-Rex cell line by doxycycline treatment. The cells were arrested in
796 mitosis by nocodazole treatment (noco.). Alternatively, they were treated with
797 thymidine (thym.) or left untreated (asy.). U2OS cells that do not express the
798 MYCBP2 fragment served as controls. (Top) Cell extracts were analyzed by
799 Western blotting. (Bottom) Quantification of relative FBXW7α signal intensity
800 was performed as described in (C).
801
802 **Figure 4. FBXO45 and MYCBP2 promote the ubiquitylation and**
803 **destabilization of FBXW7α**
804 (A) Myc-FBXO45 and HA-Ubiquitin or Myc-MYCBP2 and Flag-FBXW7α were
805 overexpressed in HEK-293T cells for 48 h. Cells were arrested in mitosis by
806 nocodazole treatment for 17 h. 4 h before harvesting, cells were treated with
807 MG132. Cell extracts were used for immunoprecipitations directed against
808 endogenous FBXW7α or against the Flag tag.
809 (B) Flag-FBXW7α FL or Flag-FBXW7αΔ106-126 were co-expressed with His-
810 Ubiquitin in HEK-293T cells. The cells were arrested in mitosis by nocodazole
811 treatment. 4 h before harvesting, cells were treated with MG132. Cell extracts
812 were prepared and α-His pull-downs were performed.
813 (C) HeLa cells were transfected with 30 nM of GL2 or FBXO45 siRNA for
814 72 h. 17 h before harvesting, the cells were treated with nocodazole. Mitotic
815 cells were collected by mitotic shake-off and further incubated with
816 nocodazole and cycloheximide (CHX). The cells were harvested at different
817 time points after the addition of cycloheximide by mitotic shake-off. Cell
818 extracts were analyzed by Western blotting. Samples were analyzed on a
819 single gel. Relative FBXW7α signal intensities were quantified.
820 (D) Flag-FBXW7α FL or Flag-FBXW7αΔ106-126 were overexpressed in
821 U2OS Flp-In-T-Rex cells by treatment with doxycycline. Cells were arrested in
822 mitosis by nocodazole treatment. Cycloheximide (CHX) was added and cells
823 were harvested at different time points after the addition of cycloheximide.
824 MG132 was added in order to inhibit the proteasome. Cell extracts were
825 analyzed by Western blotting. Relative Flag signal intensities were quantified.

826

827 **Figure 5. FBXO45 and MYCBP2 cause mitotic slippage**

828 (A) U2OS cells were treated with 250 ng/mL nocodazole. 4 h after nocodazole
829 addition, cells were analyzed by live-cell imaging. Representative images from
830 live-cell imaging are shown. Time point 0 marks induction of mitotic cell death
831 or mitotic slippage. Scale bars: 20 µm.

832 (B) U2OS cells were transfected with 30 nM of GL2 or different FBXO45
833 siRNAs for 48 h and further incubated with 250 ng/mL nocodazole.
834 Percentages of cells undergoing mitotic cell death were quantified. Cells from
835 n=3 independent experiments were analyzed. In each experiment, 50 cells
836 were quantified.

837 (C) U2OS cells were cotransfected with 40 nM of GL2 or FBXO45 siRNA and
838 an empty vector (EV) or an siRNA resistant version of Flag-FBXO45. 48 h
839 after transfection, the cells were treated with nocodazole and mitotic cell fate
840 was analyzed by live-cell imaging. Cells from n=4 independent experiments
841 were quantified.

842 (D) Expression of Flag-MYCBP2(1951-2950) was induced in U2OS cells by
843 treatment with doxycycline for 48 h. Cells were arrested in mitosis by
844 treatment with nocodazole and mitotic cell fate was analyzed by live-cell
845 imaging. Cells from n=3 independent experiments were analyzed.

846 (E) U2OS cells were transfected with 30 nM of GL2, FBXO45 or FBXW7
847 siRNA or co-transfected with FBXO45 and FBXW7 siRNA. 48 h after
848 transfection, the cells were treated with nocodazole and mitotic cell fate was
849 analyzed by live-cell imaging. Cells from n=3 independent experiments were
850 quantified.

851 For statistical analysis in (B)-(E), significance was analyzed by a two-tailed,
852 unpaired t-test. * $p<0.05$, ** $p<0.01$, n.s.: not significant.

853
854
855
856
857
858
859

860 **Table S1. Identification of FBXW7α interaction partners**

861 Selection of proteins that were specifically identified in co-immunoprecipitation
862 with Flag-FBXW7α. For each protein, the MASCOT score, mass, number of
863 significant sequences and coverage are specified.

Protein name	Score	Mass	Sign. Sequences	Coverage (%)
MYCBP2	12344	517856	164	50.3
CUL1	4091	90334	59	73.2
FBXW7	3143	80583	42	71.9
SKP1	1059	18817	12	95.7
FBXO45	908	31183	13	43.4
MYC	789	49344	9	26.2
NOTCH2	375	279081	4	4.3
MED13L	142	210603	1	2.6
NEDD8	116	8555	2	30.3
NOTCH1	97	274439	1	0.7
ARIH1	76	31920	1	6.5
RBX1	72	12722	1	13
AURORA-B	62	39977	0	6.3
MED13	56	242728	0	0.9
MTOR	50	158783	0	1.1

864

865 **Figure EV1: Related to Figure 2**

866 (A-C) The indicated Flag-tagged versions of FBXW7α were overexpressed in
867 HEK-293T cells for 24 h. Cell extracts were used for immunoprecipitations
868 with α-Flag agarose beads.

869 (D) Overview of Flag-tagged FBXW7α fragments used in (A-C). Positions of
870 N-terminal domain (blue), dimerization domain (green), F-box domain (yellow)
871 and WD40 domain (red) are indicated.

872 (E) FBXO45 specifically interacts with the α-isoform of FBXW7. Flag-
873 FBXW7α, Flag-FBXW7β or Flag-FBXW7γ were overexpressed in HEK-293T
874 cells for 24 h. FBXW7 isoforms were immunoprecipitated by their Flag tags.
875 Immunoprecipitates were analyzed by Western blotting.

876

877 **Figure EV2: Related to Figure 2**

878 (A) Overview of MYCBP2 fragments used in (B). Positions of RCC1-like
879 domain (blue), PHR domains (green), MYC-binding domain (yellow) and
880 RING domain (red) are shown.

881 (B) FBXW7α and FBXO45 interact with the central domain of MYCBP2. The
882 indicated Flag-tagged MYCBP2 fragments were overexpressed in HEK-293T
883 cells for 24 h. Cell extracts were used for α-Flag immunoprecipitations.
884 (C) Flag-FBXW7α was overexpressed in HEK-293T cells for 24 h. 4 h before
885 harvesting, the cells were treated with 100 nM BI2536. Cell extracts were
886 used for α-Flag immunoprecipitations.
887 (D) Flag-FBXW7α and GFP-PLK2 were co-expressed in HEK-293T cells for
888 24 h. Cell extracts were used for α-Flag immunoprecipitations.
889
890 **Figure EV3: Related to Figure 3**
891 (A) HeLa cells were transfected with 30 nM FBXO45 and MYCBP2 siRNAs for
892 72 h. GL2 siRNA was used as a control. The cells were arrested in mitosis by
893 nocodazole (noco.) treatment for 17 h and collected by a mitotic shake-off.
894 Alternatively, mitotic cells were enriched after a release from a double-
895 thymidine block (thym. release), followed by a mitotic shake-off when the cells
896 reached the mitotic peak. Mitotic cells were compared with an asynchronous
897 (asy.) cell population. (Top) Cell extracts were analyzed by Western blotting.
898 (Bottom) A quantification of relative FBXW7α signal intensities is shown.
899 Relative FBXW7α signals in the GL2 controls were set to 1. Average signal
900 intensities and standard deviations from n=5 experiments were calculated.
901 Statistical significance was analyzed by a two-tailed, unpaired t-test with
902 unequal variance. * $p<0.05$; n.s.: not significant.
903 (B) Characterization of MYCBP2 siRNAs used in this study. HeLa cells were
904 transfected with 30 nM of GL2 or MYCBP2 siRNAs for 72 h. Cell extracts
905 were analyzed by Western blotting.
906 (C) HeLa cells were transfected with 30 nM of GL2 siRNA, three different
907 FBXO45 siRNAs or two different MYCBP2 siRNAs for 72 h. In addition, the
908 cells were treated with nocodazole for 17 h before they were collected by a
909 mitotic shake-off. (Top) Cell extracts were analyzed by Western blotting.
910 (Bottom) Relative FBXW7α signal intensities were quantified. Relative signal
911 intensity in the GL2 control was set to 1. Average signal intensities and
912 standard deviations from n=3 experiments were calculated. Statistical
913 significance was analyzed by a two-tailed, unpaired t-test with unequal
914 variance. * $p<0.05$; ** $p<0.01$.

915 (D) U2OS cells were transfected with 30 nM of GL2 or FBXO45 siRNA for
916 72 h. 17 h before harvesting, they were arrested in mitosis by treatment with
917 nocodazole. Mitotic cells were harvested by mitotic shake-off. Cell extracts
918 were analyzed by Western blotting.
919 (E-I) HeLa cells were transfected with 30 nM of GL2 or FBXO45 siRNA for
920 72 h. 17 h before harvesting, they were arrested in mitosis by treatment with
921 nocodazole (noco., (E)), Taxol (F), vincristine (vincr., (G)), STLC (H) or
922 BI2536 (I). Mitotic cells were harvested by mitotic shake-off. Cell extracts
923 were prepared and analyzed by Western blotting. Relative FBXW7α signal
924 intensities were quantified.
925
926 **Figure EV4: Related to Figure 5**
927 (A) U2OS cells were transfected with 30 nM of GL2 or FBXO45 siRNA for
928 48 h and further incubated with 1 μM Taxol. Percentages of cells undergoing
929 mitotic cell death were quantified. Cells from n=4 independent experiments
930 were analyzed. In each experiment, 50 cells were quantified. Statistical
931 significance was analyzed by a two-tailed, unpaired t-test. * $p<0.05$.
932 (B) U2OS cells were transfected with 30 nM of GL2 or FBXO45 siRNA for
933 48 h and further incubated with 1 μM vincristine. Percentages of cells
934 undergoing mitotic cell death were quantified. Cells from n=4 independent
935 experiments were analyzed. In each experiment, 50 cells were quantified.
936 Statistical significance was analyzed by a two-tailed, unpaired t-test. * $p<0.05$.
937 (C) U2OS cells were transfected with 30 nM of GL2 or two different MYCBP2
938 siRNAs for 48 h and further incubated with 250 ng/mL nocodazole.
939 Percentages of cells undergoing mitotic cell death were quantified. Cells from
940 n=4 independent experiments were analyzed. In each experiment, 50 cells
941 were quantified. Statistical significance was analyzed by a two-tailed,
942 unpaired t-test. * $p<0.05$.
943 (D) HeLa H2B-RFP/GFP-α-tubulin cells were transfected with 30 nM of GL2
944 or FBXO45/MYCBP2 siRNAs for 72 h. They were released from a thymidine
945 block and their mitotic progression was analyzed and quantified by live-cell
946 imaging.
947
948

949 **Video S1: Related to Figure 5**

950 Exemplary video of a U2OS cell undergoing mitotic cell death upon prolonged
951 mitotic arrest. Mitotic arrest was caused by treatment with nocodazole.

952

953 **Video S2: Related to Figure 5**

954 Exemplary video of a U2OS cell undergoing mitotic slippage upon prolonged
955 mitotic arrest. Mitotic arrest was caused by treatment with nocodazole.

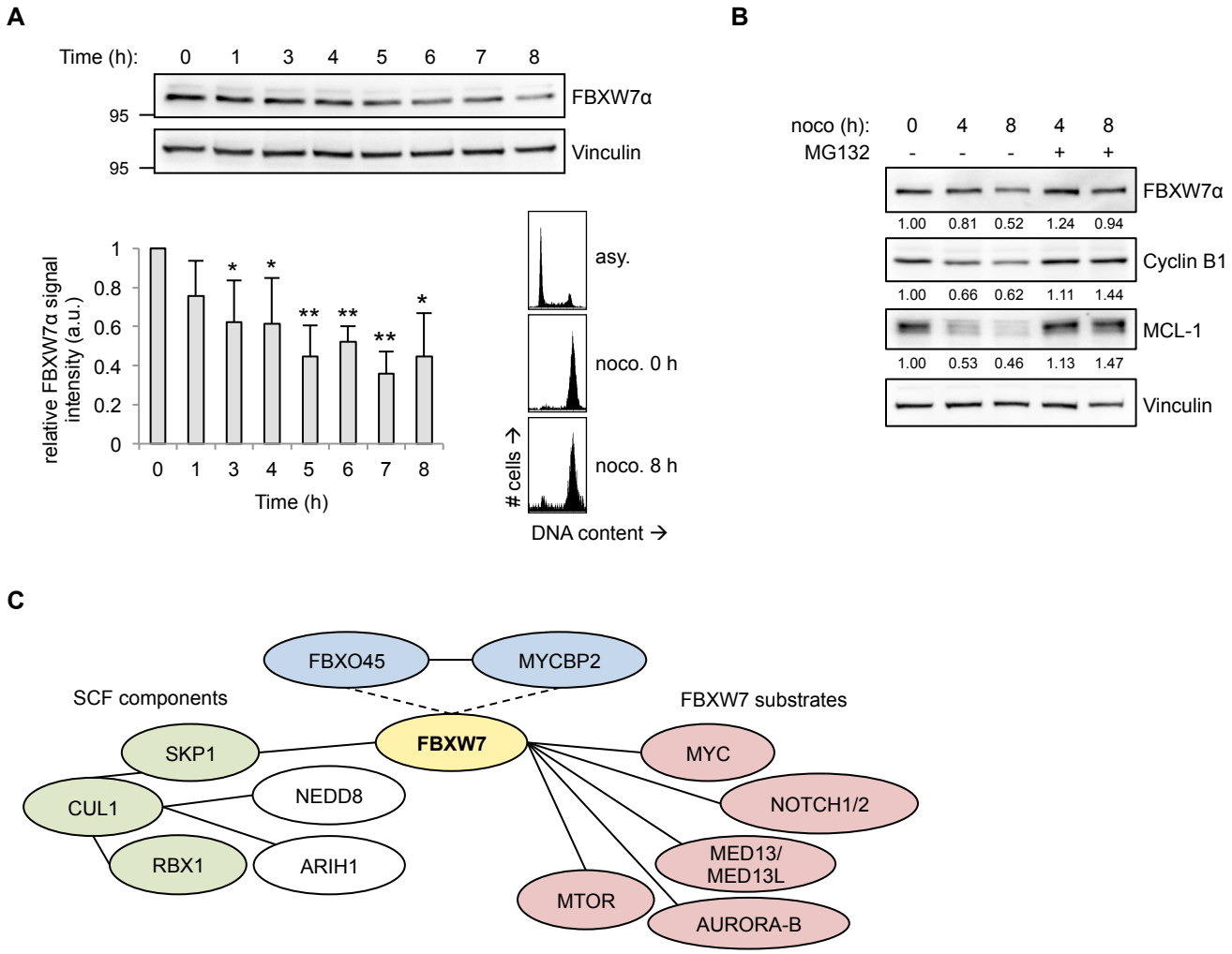
A
Time (h): 0 1 3 4 5 6 7 8
95
FBXW7α
95
Vinculin
relative FBXW7α signal intensity (a.u.)
1
0.8
0.6
0.4
0.2
0
0 1 3 4 5 6 7 8
Time (h)
asy.
noco. 0 h
noco. 8 h
cells →
DNA content →
B
noco (h): 0 4 8 4 8
MG132 - - - + +
FBXW7α
1.00 0.81 0.52 1.24 0.94
Cyclin B1
1.00 0.66 0.62 1.11 1.44
MCL-1
1.00 0.53 0.46 1.13 1.47
Vinculin
C
FBXO45
MYCBP2
SCF components
FBXW7 substrates
SKP1
FBXW7
MYC
CUL1
NEDD8
NOTCH1/2
RBX1
ARIH1
MED13/
MED13L
MTOR
AURORA-B

Figure 1

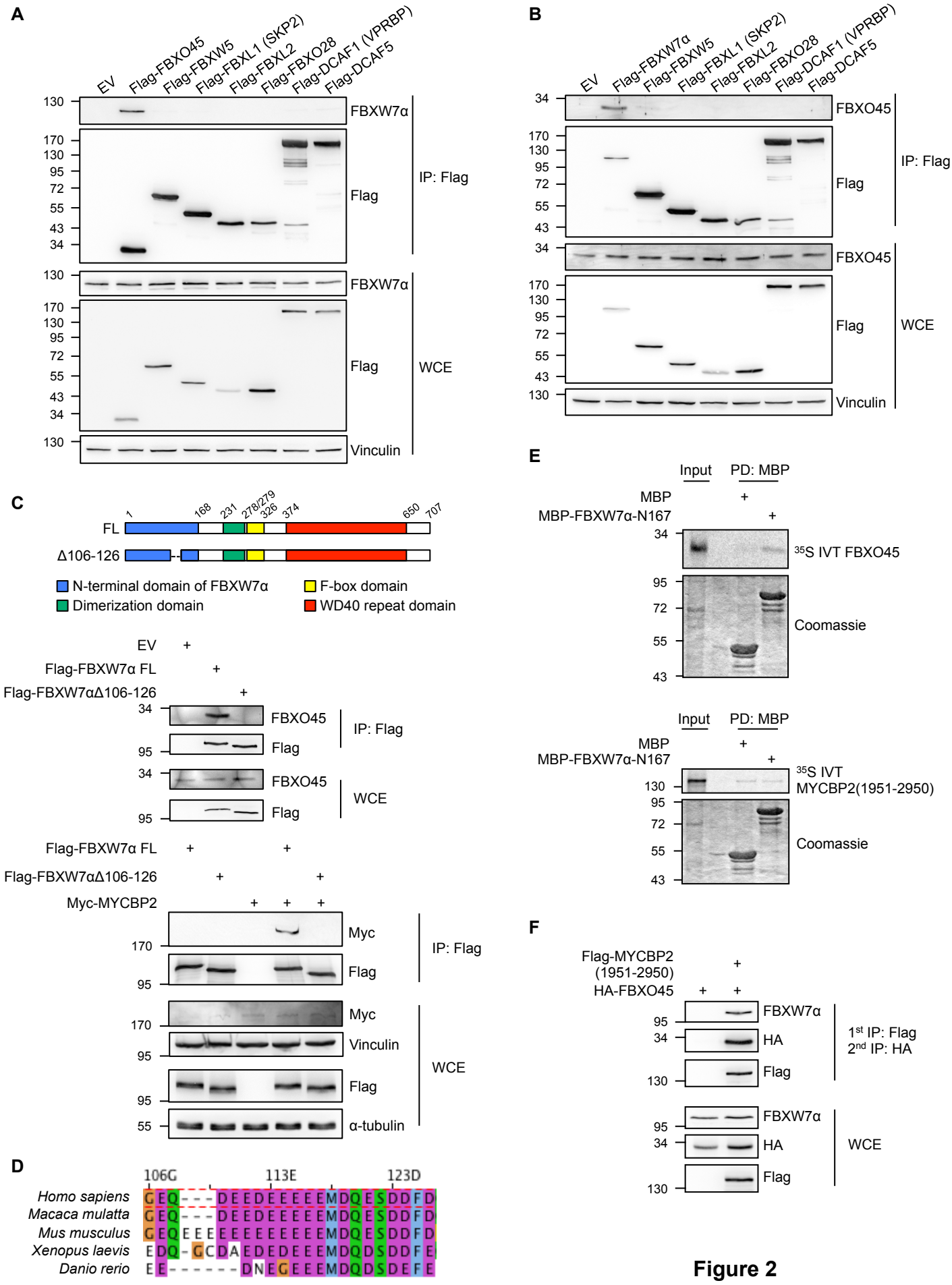
A
EV
Flag-FBXO45
Flag-FBXW5
Flag-FBXL1 (SKP2)
Flag-FBXL2
Flag-FBXO28
Flag-DCAF1 (VPRBP)
Flag-DCAF5
FBXW7α
Flag
IP: Flag
WCE
Vinculin
B
Flag-FBXW7α
FBXO45
C
FL
Δ106-126
N-terminal domain of FBXW7α
F-box domain
Dimerization domain
WD40 repeat domain
Flag-FBXW7α FL
Flag-FBXW7αΔ106-126
Myc-MYCBP2
Myc
α-tubulin
D
106G
113E
123D
Homo sapiens
Macaca mulatta
Mus musculus
Xenopus laevis
Danio rerio
E
Input
PD: MBP
MBP
MBP-FBXW7α-N167
35S IVT FBXO45
Coomassie
35S IVT MYCBP2(1951-2950)
F
Flag-MYCBP2 (1951-2950)
HA-FBXO45
1st IP: Flag
2nd IP: HA

Figure 2

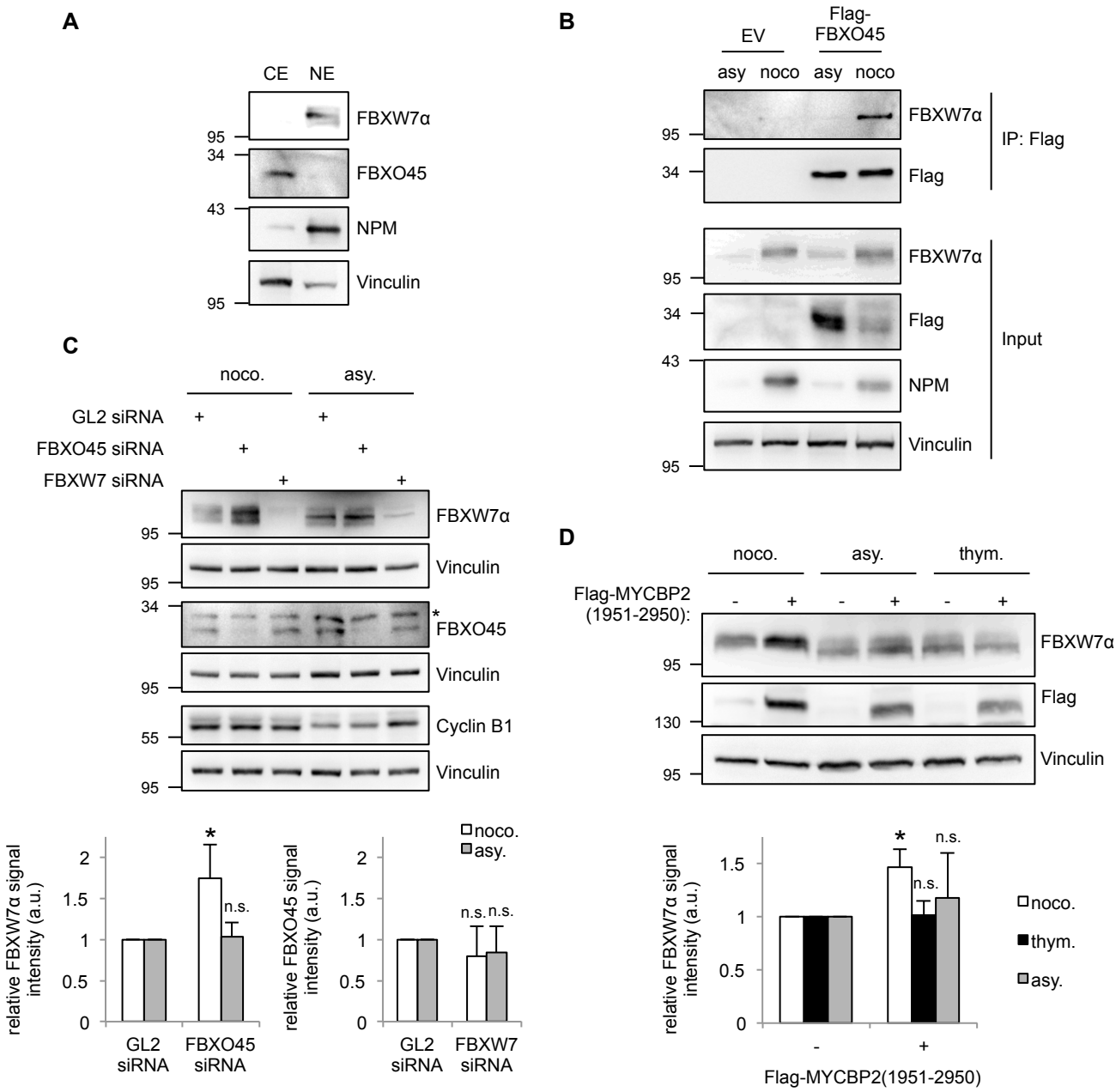
A
CE
NE
FBXW7α
FBXO45
NPM
Vinculin
95
34
43
95
B
EV
Flag-FBXO45
asy
noco
asy
noco
FBXW7α
Flag
IP: Flag
FBXW7α
Flag
NPM
Vinculin
Input
95
34
43
95
C
noco.
asy.
GL2 siRNA
FBXO45 siRNA
FBXW7 siRNA
FBXW7α
Vinculin
FBXO45
Vinculin
Cyclin B1
Vinculin
95
95
34
95
55
95
relative FBXW7α signal intensity (a.u.)
relative FBXO45 signal intensity (a.u.)
noco.
asy.
n.s.
n.s.
n.s.
GL2 siRNA
FBXO45 siRNA
GL2 siRNA
FBXW7 siRNA
D
noco.
asy.
thym.
Flag-MYCBP2 (1951-2950):
FBXW7α
Flag
Vinculin
95
130
95
relative FBXW7α signal intensity (a.u.)
n.s.
n.s.
noco.
thym.
asy.
Flag-MYCBP2(1951-2950)

Figure 3

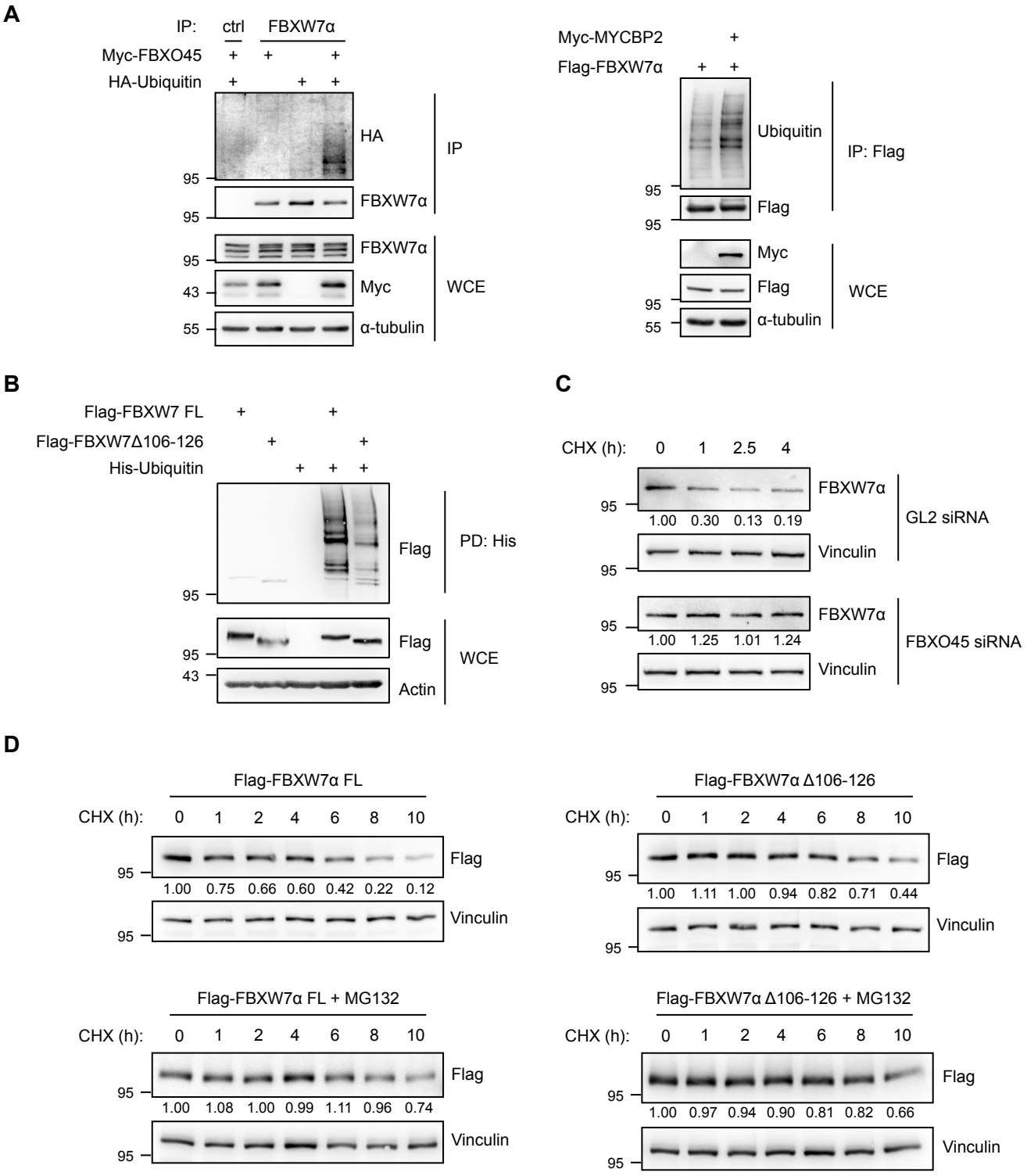
A
IP: ctrl FBXW7α
Myc-FBXO45 + + +
HA-Ubiquitin + + +
HA
FBXW7α
IP
95
95
FBXW7α
Myc
α-tubulin
WCE
95
43
55
Myc-MYCBP2 +
Flag-FBXW7α + +
Ubiquitin
Flag
IP: Flag
95
95
Myc
Flag
α-tubulin
WCE
95
55
B
Flag-FBXW7 FL + +
Flag-FBXW7Δ106-126 + +
His-Ubiquitin + + +
Flag
PD: His
95
Flag
Actin
WCE
95
43
C
CHX (h): 0 1 2.5 4
FBXW7α
1.00 0.30 0.13 0.19
Vinculin
GL2 siRNA
95
95
FBXW7α
1.00 1.25 1.01 1.24
Vinculin
FBXO45 siRNA
95
95
D
Flag-FBXW7α FL
CHX (h): 0 1 2 4 6 8 10
Flag
95
1.00 0.75 0.66 0.60 0.42 0.22 0.12
Vinculin
95
Flag-FBXW7α Δ106-126
CHX (h): 0 1 2 4 6 8 10
Flag
95
1.00 1.11 1.00 0.94 0.82 0.71 0.44
Vinculin
95
Flag-FBXW7α FL + MG132
CHX (h): 0 1 2 4 6 8 10
Flag
95
1.00 1.08 1.00 0.99 1.11 0.96 0.74
Vinculin
95
Flag-FBXW7α Δ106-126 + MG132
CHX (h): 0 1 2 4 6 8 10
Flag
95
1.00 0.97 0.94 0.90 0.81 0.82 0.66
Vinculin
95

Figure 4

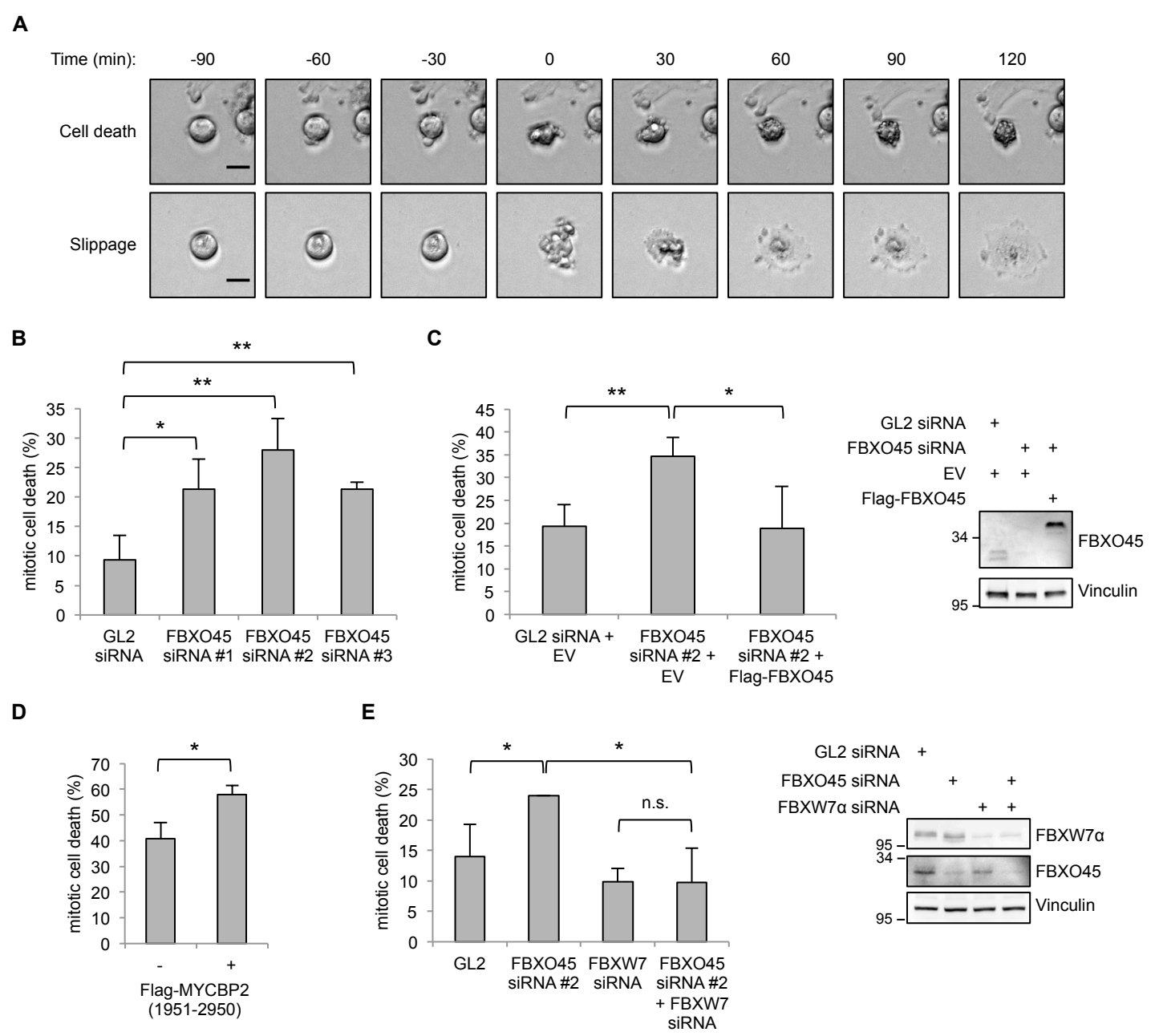
A
Time (min):
-90
-60
-30
0
30
60
90
120
Cell death
Slippage
B
mitotic cell death (%)
GL2 siRNA
FBXO45 siRNA #1
FBXO45 siRNA #2
FBXO45 siRNA #3
C
mitotic cell death (%)
GL2 siRNA + EV
FBXO45 siRNA #2 + EV
FBXO45 siRNA #2 + Flag-FBXO45
GL2 siRNA
FBXO45 siRNA
EV
Flag-FBXO45
FBXO45
Vinculin
D
mitotic cell death (%)
Flag-MYCBP2 (1951-2950)
E
mitotic cell death (%)
GL2
FBXO45 siRNA #2
FBXW7 siRNA
FBXO45 siRNA #2 + FBXW7 siRNA
n.s.
GL2 siRNA
FBXO45 siRNA
FBXW7α siRNA
FBXW7α
FBXO45
Vinculin

Figure 5

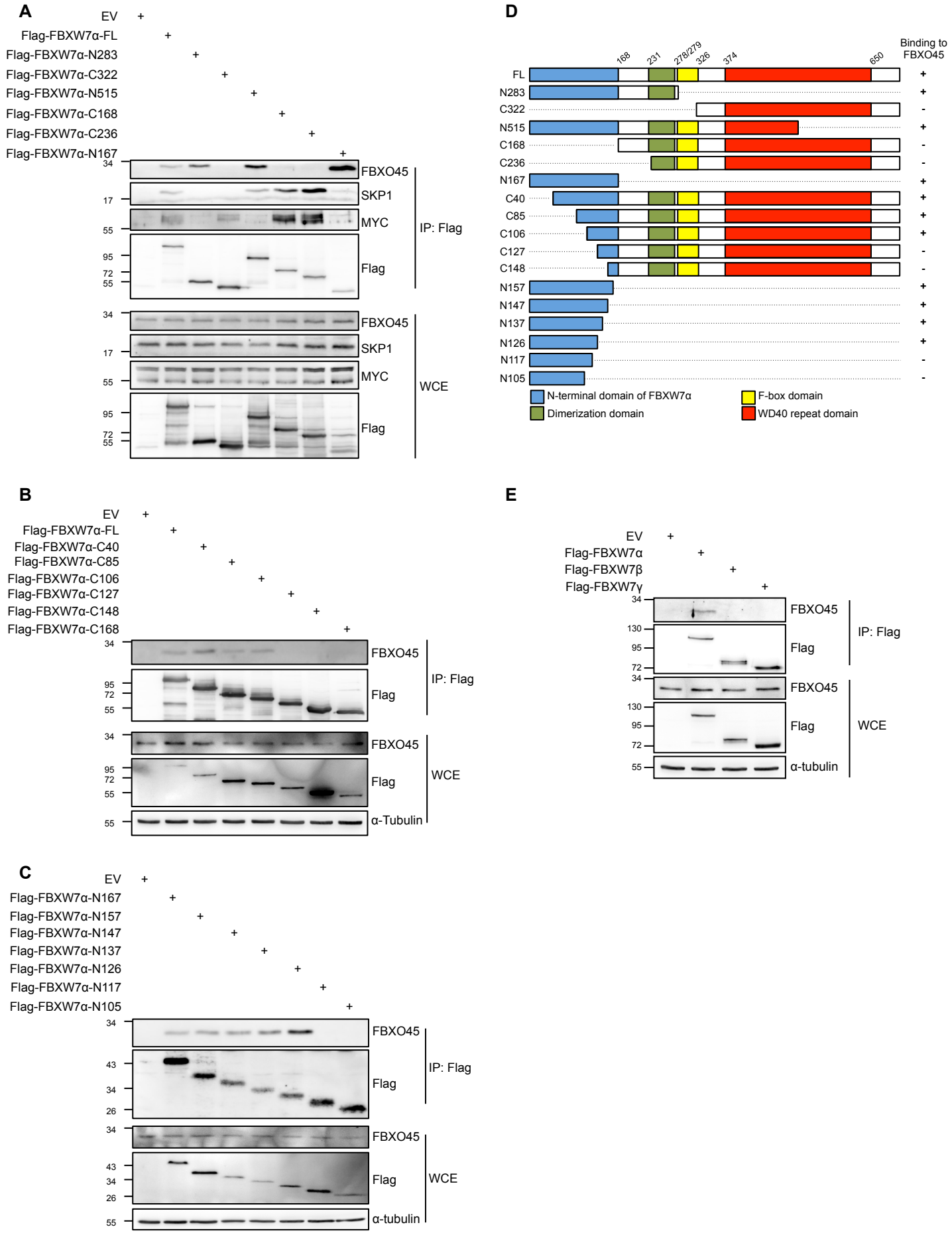

Figure EV1: Related to Figure 2

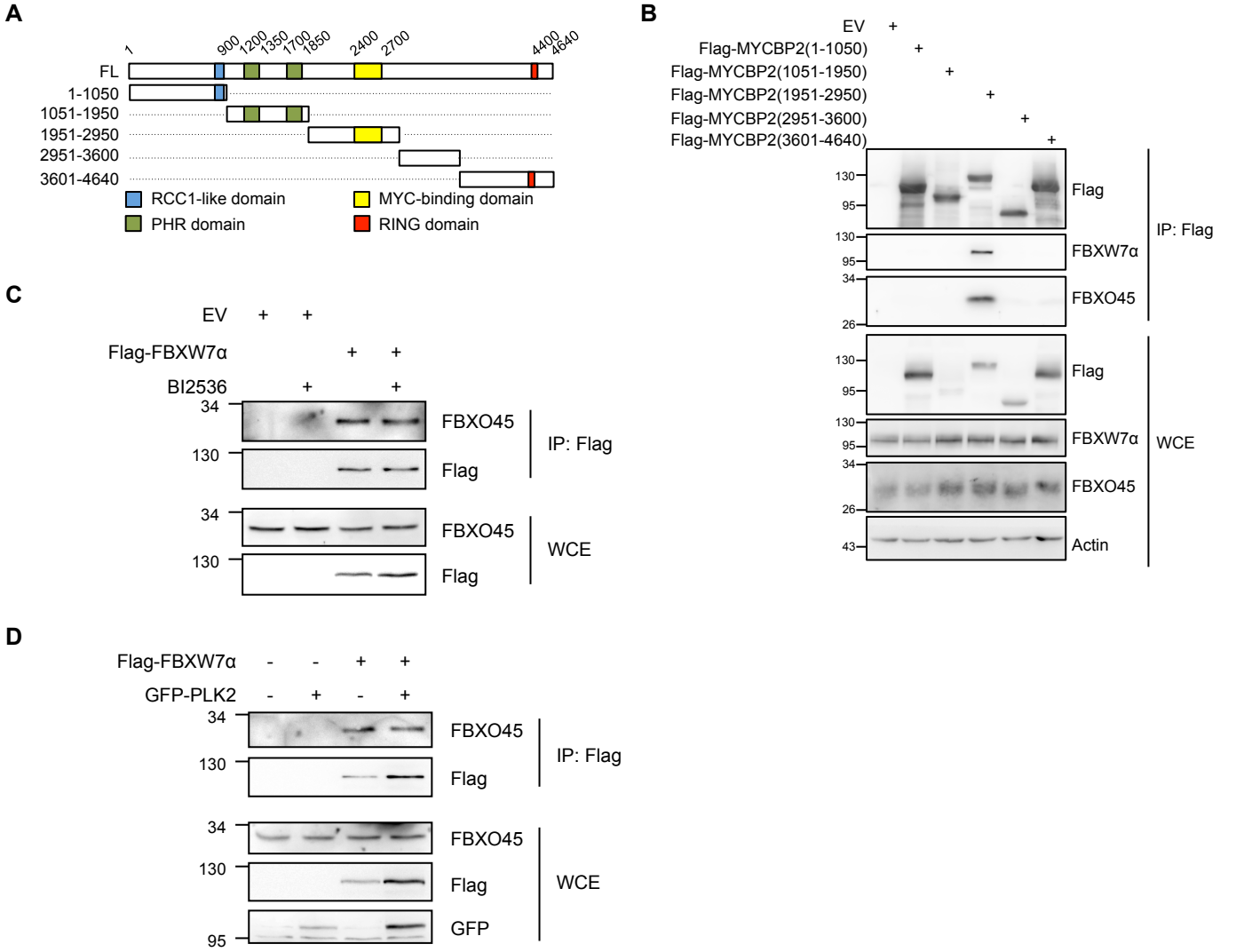

Figure EV2: Related to Figure 2

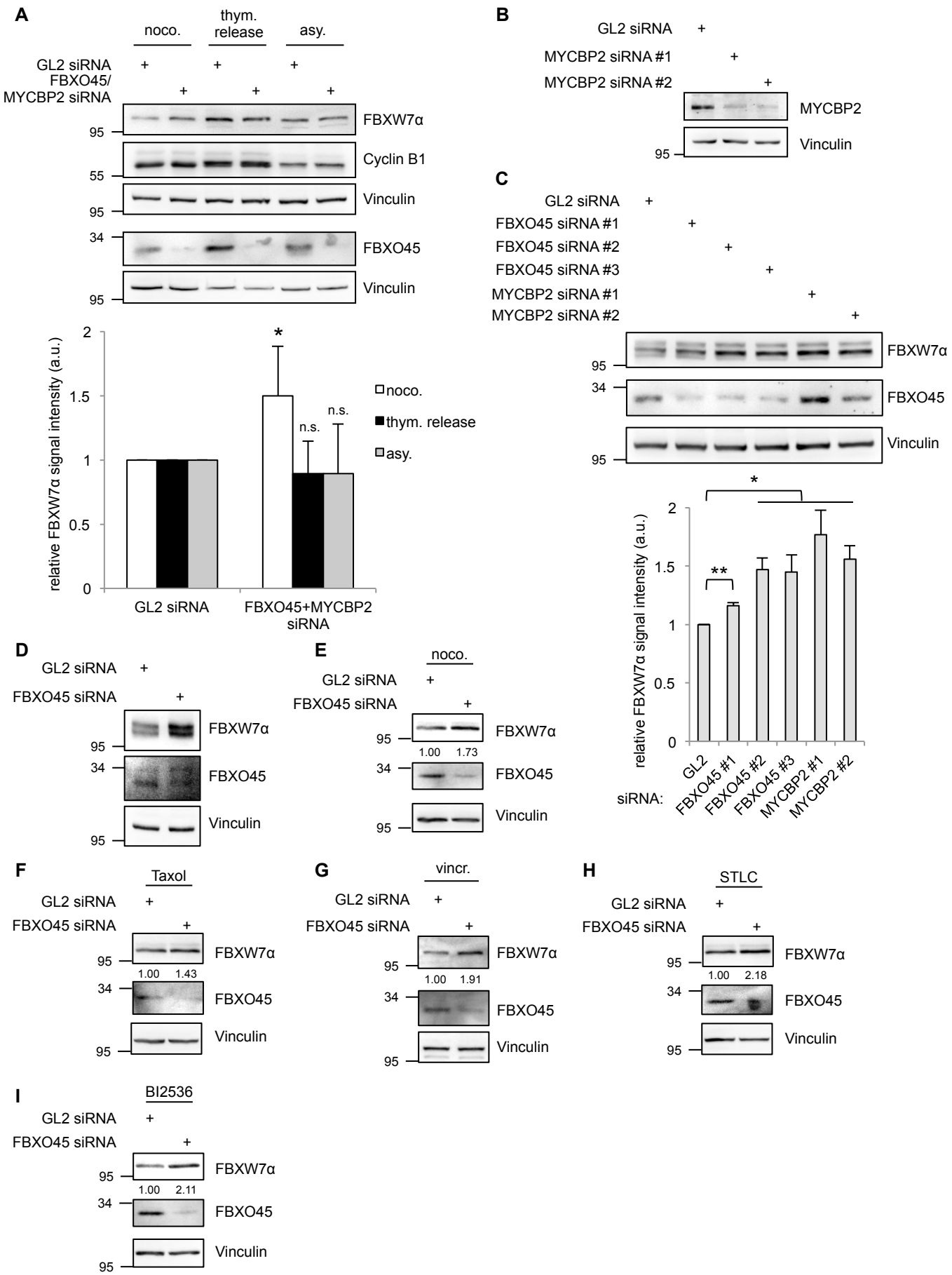

Figure EV3: Related to Figure 3

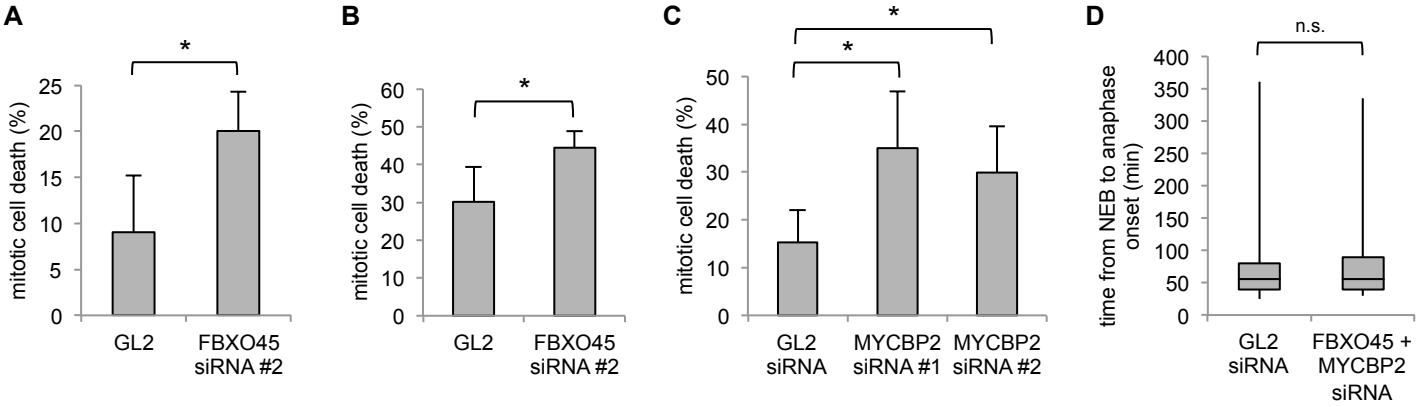

Figure EV4: Related to Figure 5